hexagon:2611.00907v1

# A length-minimizing curve with discontinuous velocity in a smooth sub-Riemannian structure

Bangjie Wang Igor Zelenko

November 21, 2026

**Abstract**

We construct a smooth, bracket-generating rank-two sub-Riemannian structure near the origin in $\mathbb{R}^6$ and a length-minimizing curve whose arclength velocity is discontinuous at an interior point. This strictly abnormal extremal trajectory is differentiable there and has a unique horizontal tangent. The limiting velocity directions from the right form an arc of positive length in the horizontal unit circle at that point, with the tangent direction as one endpoint. Short subarcs uniquely minimize length up to reparametrization. A sequence of smooth Hamilton–Jacobi subsolutions yields finite Hilbert invariant-integral comparisons with errors tending to zero. This gives a negative answer to the general question whether length minimizers in smooth sub-Riemannian structures must have continuous arclength velocity. No smooth local diffeomorphism takes the distribution germ at the origin to a real-analytic distribution. In particular, it admits no polynomial frame in any smooth local coordinates. We also announce a sharp 1/2-Hölder estimate for the arclength velocity of minimizers in rank-two Carnot groups of step at most five. We propose a proof of this estimate in a separate manuscript. The step-five example announced by Cavallucci, Le Donne and Nicolussi Golo has precisely this exponent at an interior point.

*2020 Mathematics Subject Classification.* Primary 53C17; Secondary 49K15, 49L12, 49N60, 53C22.

*Keywords.* Sub-Riemannian geometry; strictly abnormal extremal trajectories; regularity of length minimizers; discontinuous velocity; Hamilton–Jacobi subsolutions.

## Contents

**1 Introduction** **3**

**2 The curve and its horizontal equations** **7**
2.1 Horizontal lifts and length . . . . . 7

**3 A smooth transition and its Hamilton–Jacobi subsolution** **9**
3.1 The transition and its horizontal lift . . . . . 9
3.2 Bracket generation and unique minimality . . . . . 10

**4 From a transition to accumulating pulses** **12**
4.1 Returning to the clock axis . . . . . 12
4.2 Preserving the reference phase equations . . . . . 13
4.3 Why the observations must be localized . . . . . 14

**5 Recovering the separate cell integrals** **14**

**6 The complete construction** **16**
6.1 Scales and cells . . . 16
6.2 The localized profile and its density . . . 17
6.3 Gap tests, observation powers, and accumulated values . . . 18
6.4 The phase coefficients and the frame . . . 19
6.5 The reference and its endpoints . . . 20

**7 Length minimization with ODE endpoint constraints** **20**
7.1 The endpoint problem . . . 20

**8 Smoothness, brackets, and velocity limits** **21**
8.1 Estimates for the rescaled transition . . . 21
8.2 Localization and pulse energy . . . 23
8.3 Smooth extension of the coefficients . . . 25
8.4 Bracket generation . . . 27
8.5 Differentiability of the curve and its velocity limits . . . 27

**9 Comparison deficits and clock reversals** **29**
9.1 The reference tail and the initial deficit . . . 29
9.2 Finite comparisons and the clock estimate . . . 30

**10 Recovering cell integrals from the endpoints** **30**
10.1 The nonnegative rate and its derivative . . . 30
10.2 A one-sided cell observation . . . 31
10.3 Size of the observation errors . . . 32

**11 From an integral to a spatial bound** **33**
11.1 Bounds for the quartic density . . . 33
11.2 A peak estimate in arclength . . . 34

**12 Hamilton–Jacobi subsolutions and finite length comparisons** **36**
12.1 A smooth Hamilton–Jacobi subsolution on a cell . . . 36
12.2 A sequence of finite Hamilton–Jacobi comparisons . . . 37
12.3 The Hilbert invariant integral for the lifted endpoints . . . 38

**13 Minimality by induction over the cells** **39**
13.1 The counterexample . . . 41

**14 Further properties and equiregular lifting** **41**
14.1 Relation to regularity theorems . . . 45
14.2 Equiregular lifting . . . 45

# 1 Introduction

Let $M$ be a smooth manifold and let $\mathcal{D} \subset TM$ be a smooth rank-two distribution with a smooth inner product. We assume that iterated Lie brackets of local sections of $\mathcal{D}$ span $T_qM$ at every $q \in M$. In an orthonormal frame $X_1, X_2$, an absolutely continuous curve $\gamma$ is horizontal if

$$\dot{\gamma} = u_1 X_1(\gamma) + u_2 X_2(\gamma) \quad \text{a.e.}, \qquad L(\gamma) = \int |u(s)|\, ds.$$

Its control $u = (u_1, u_2)$ has norm one almost everywhere in an arclength parametrization. A length minimizer realizes the infimum of length over all horizontal curves joining its endpoints.

By the Pontryagin Maximum Principle [1, 2, 21], every arclength-parametrized length minimizer admits a special lift to the cotangent bundle $T^*M$, called a (Pontryagin) *extremal*. We call the projection of an extremal to $M$ an *extremal trajectory*. In the equivalent fixed-time energy problem, an extremal is *normal* if the scalar multiplier $\lambda_0$ of the energy functional $\frac{1}{2}\int |u|^2\, ds$ is nonzero and *abnormal* if $\lambda_0 = 0$. A trajectory can admit lifts of both types.

Normal extremal trajectories are smooth in arclength because they are projections of integral curves of the smooth sub-Riemannian Hamiltonian vector field. In the Riemannian case there are no abnormal extremals (an abnormal lift would require a nonzero covector annihilating the entire tangent space), so every length minimizer is a smooth geodesic in its arclength parametrization. In sub-Riemannian geometry, abnormal extremals and their projections can have discontinuous velocity when the projection is parametrized by arclength.

The question whether every arclength-parametrized sub-Riemannian length minimizer is smooth goes back at least to Strichartz's 1986 paper and his 1989 correction [24, 25]. In 1994 Montgomery constructed a smooth length minimizer admitting only abnormal lifts [16]. In 1995, Agrachev and Sarychev [3] and Liu and Sussmann [14] gave sufficient conditions for abnormal extremal trajectories of rank-two distributions to be locally length minimizing. Zelenko's 1999 criterion concerns the $W^{1,\infty}$-rigidity of nonregular abnormal extremal trajectories, namely their local isolation among fixed-endpoint horizontal curves up to reparametrization [28].[1] Montgomery explicitly posed the general smoothness question in his 2002 book [17, Problem 10.1]. Monti surveyed the problem in 2014 [18].

Hakavuori and Le Donne's 2016 no-corner theorem rules out linearly independent one-sided arclength velocities at an interior point of a length minimizer [10]. In 2018, Monti, Pigati and Vittone proved that at every interior point of a length minimizer at least one blow-up in the nilpotent approximation is a straight horizontal line [19, Theorem 1.1]. This gives a limiting direction along a sequence of scales and leaves open whether the velocity is continuous. Under additional hypotheses, $C^1$ regularity was proved for rank-two structures of step at most four in 2020 [4], for real-analytic three-dimensional structures in 2022 [5], and for real-analytic equiregular metabelian rank-two structures in work first circulated in 2024 [13].

In January 2025, Chitour, Jean, Monti, Rifford, Sacchelli, Sigalotti and Socionovo gave a negative answer to the general smoothness question [7, Theorem 1.1]. In a polynomial rank-two structure on $\mathbb{R}^3$, they proved that the arc, written in clock-first coordinates as $(t, t^{5/2}, 0)$, $0 \le t \le \varepsilon$, minimizes length for sufficiently small $\varepsilon > 0$. Its arclength parametrization is $C^2$ and fails to be $C^3$ at the endpoint $t = 0$. In March 2026, Rossi, Schiavoni Piazza and Socionovo exhibited the same loss of regularity at an interior point in a real-analytic structure of Martinet type. Their minimizing arcs coincide up to that point and then branch. They also obtained nonsmooth branching minimizers in Carnot groups [22, Theorems 1.1–1.3].

[1] In rank two, the regular abnormal extremals of Liu and Sussmann [14] are precisely those that satisfy the strong generalized Legendre–Clebsch condition used by Agrachev and Sarychev [3], after choosing the sign of the covector. An extremal is *nonregular* if this condition degenerates at some point along it.

In October 2026, Cavallucci, Le Donne and Nicolussi Golo constructed a $C^1$ minimizer in a polynomial rank-two structure on $\mathbb{R}^4$ whose arclength parametrization has no second derivative at an interior point. Its planar projection, in clock–space order, is $(t, t\sqrt{|t|})$, and the proof of minimality uses an approximate calibration depending on the competitor [6, Theorem A]. Near $t = 0$ its arclength velocity is $1/2$-Hölder and fails to be $\alpha$-Hölder for every $\alpha > 1/2$. The authors describe a minimizing lift to a rank-two Carnot group of step five. More generally, for every integer $n \geq 0$ they announce a rank-two Carnot group of step at most $2n + 5$ with a minimizer whose arclength velocity has sharp Hölder exponent $\beta_n = 1/(2(n + 1))$ at an interior point [6, Theorem B]. They defer the details of the Carnot lift and the proof of Theorem B to a companion paper. Since $\beta_n \to 0$, for every $\alpha > 0$ the announced family contains a $C^1$ minimizer whose velocity fails to be $\alpha$-Hölder, with the group depending on $\alpha$.

It remained open whether the arclength velocity of every sub-Riemannian length minimizer must be continuous at interior points [6]. The following theorem gives a six-dimensional counterexample.

**Theorem 1.** *There exists a smooth, bracket-generating rank-two sub-Riemannian structure on an open subset of $\mathbb{R}^6$ admitting a strictly abnormal extremal trajectory that uniquely minimizes length between its endpoints and has discontinuous arclength velocity at an interior point.*

The frame in (6.24) defines the distribution $\mathcal{D}_a$ and metric $g_a$ of Theorem 1; its minimizing reference arc is $\Gamma_a$ in (6.25). Section 6 specifies all their coefficients. The metric measures planar length, while the auxiliary endpoints exclude shortenings. The proof includes competitors whose clock pauses or reverses.

Section 14 proves the following additional properties of the example (Proposition 14.1).

- No smooth local change of coordinates makes the distribution real-analytic near the origin. In particular, it has no polynomial horizontal frame in any smooth local coordinates.
- At the origin, iterated brackets first span the tangent space at length 51. Even the dimension spanned by the horizontal fields and their first brackets varies nearby.
- The arc is smooth away from the origin and differentiable there. Its rescaled arcs converge to a single horizontal line.
- Small translations of the arclength control are small in $L^p$, with Hölder exponent $1/p$ for $1 < p < \infty$.

Proposition 14.5 also gives a higher-dimensional example in an equiregular structure, where the dimensions of the spans of brackets of each bounded length are constant. Every lift considered there is intrinsically nonanalytic as a sub-Riemannian structure. The free lift can also be chosen so that its underlying distribution has no real-analytic realization (Subsection 14.2).

Zelikin and Lokutsievskiy [30] construct chattering shortest paths for polyhedral sub-Finsler norms. Here the horizontal norm is induced by a positive-definite quadratic form, so their examples concern a different class of length functionals.

**Open regularity questions.** The distribution of Theorem 1 admits no real-analytic realization near the origin (Proposition 14.1(i)). Whether every length minimizer parametrized by arclength has continuous velocity at interior points remains open for real-analytic sub-Riemannian structures in general, for structures given by polynomial orthonormal frames, and for left-invariant sub-Riemannian metrics on Carnot groups [6, 22].

In our forthcoming paper [27] we propose a proof that in every rank-two Carnot group of step at most five, the arclength velocity of each length minimizer is locally $1/2$-Hölder, up to and including the endpoints. This bound matches the step-five example announced by Cavallucci, Le Donne and

Nicolussi Golo in October 2026 [6], whose velocity has sharp Hölder exponent $1/2$ at an interior point. For $n \geq 1$, we conjecture that the arclength velocity of every length minimizer in a rank-two Carnot group of step at most $2n+5$ is locally $\beta_n$-Hölder, where $\beta_n = 1/(2(n+1))$. This would give the matching lower bounds for the examples announced in [6, Theorem B]. For every step bound above five, starting with step six, the optimal exponent guaranteed for all rank-two Carnot minimizers remains open.

**Outline of the construction.** The problem is to preserve a fixed change of velocity on smaller and smaller pieces of a minimizing curve. A planar graph can easily have this behavior, but its curved pieces can be shortened. We therefore keep planar length as the metric and use auxiliary endpoint coordinates to make those shortenings inadmissible. The construction proceeds as follows.

First choose one smooth increasing *transition*: a whole-line graph approaching two constant spatial levels (Section 3, (3.1)). Its shape and quartic potential are chosen together so that a smooth Hamilton–Jacobi subsolution is sharp on the graph ((3.5)). Integrating its exact differential is the associated Hilbert invariant-integral comparison. This gives minimality even when a competitor's clock reverses.

Next place scaled copies in disjoint *cells* accumulating at zero, and return the graph to the clock axis between them. The graph on one cell is a *pulse*; the intervening interval is a *gap* (Definition 6.1). The narrow transition window has width of order $h_n$, while its amplitude is $b_n = ah_n$ with a fixed small $a > 0$ ((6.9)–(6.10)). Hence its slope does not shrink. Nevertheless $h_n/t_n \to 0$, so the accumulated graph is differentiable at zero with horizontal tangent (Figure 1). The wider return scale $\ell_n \gg h_n$ makes the return slopes small. Localization breaks the original stationary equation; the linear correction in (6.16) restores it, and the quadratic correction provides the positive margin needed for a cell subsolution.

The coordinate $W$ records a weighted sum of cell integrals. Opposite changes in different cells can cancel in that sum. The coordinate $Z$ therefore tests the accumulated value in each gap through a nonnegative square ((5.1)). With an increasing clock, its zero endpoint increment recovers each cell integral exactly (Proposition 5.1). The phase states $r, \xi$ keep $\xi = 0$ on the reference and supply bracket directions; their equations and the powers $\xi^6, \xi^{10}$ are motivated in Sections 4–6. The full distribution and the reference are (6.24) and (6.25).

For an arbitrary competitor, signed clock motion can cancel those nonnegative tests. We measure this possibility by the fixed quantity $\mathfrak{B} = \int (1-2u_t)_+ \, ds$ ((9.1)), where $u_t$ is the clock component of the planar unit velocity. The endpoint tests recover each cell integral with an error of order $\mathfrak{B}^{11/2}$ (Proposition 10.2). Before using the next subsolution, the recovered integral and the spatial energy bound confine every visit to that cell (Lemma 11.4). This is necessary because the subsolution is initially available only on a bounded spatial band.

Finally sum the subsolutions on finitely many cells. Their Hamilton–Jacobi inequality and Hilbert interpretation give (12.12); the same whole competitor is used at every stage. The old bound on $\mathfrak{B}$ absorbs the new observation error and improves the bound to the next pulse scale (Lemma 13.1). The reference tail and the remaining errors tend to zero in (13.4). Vanishing of the nonnegative deficits identifies the reference. This proof uses a sequence of smooth finite subsolutions, without requiring a limiting potential.

**Organization.** Section 2 displays the curve and its horizontal equations. Section 3 gives a complete six-dimensional smooth model, including bracket generation and unique minimality. Section 4 explains the corrections needed to assemble accumulating pulses; Section 5 establishes the separate integral constraints supplied by the gap tests. Section 6 specifies all coefficients and the reference. Section 7 states the minimality of this construction. Section 8 proves smoothness, bracket generation, and the velocity assertions. Sections 9–13 prove minimality using endpoint observations, spatial

confinement, and a sequence of finite Hamilton–Jacobi comparisons with their Hilbert invariant-integral interpretation. Section 14 proves the further properties and gives the equiregular lifting.

**Conventions and notation.** Planar coordinates are ordered as $(t, x)$, with $t$ the clock. The horizontal frame lifts $\partial_t, \partial_x$ in that order, so its controls are the planar velocities. We use bold letters for two-dimensional vectors. Integrals along competitors are in arclength unless stated otherwise; integrals written with $dt$ are signed and include the clock velocity.

**Acknowledgments.** We thank Boris Doubrov for discussions about the distinction between smooth and real-analytic sub-Riemannian structures. These discussions led us to conjecture how the sharp Hölder exponent for the arclength velocities of minimizers in rank-two Carnot groups depends on the step. They also led to our proof that the sharp exponent at step five is $1/2$, which we present in our forthcoming paper [27].

**AI disclosure and verification status.** *Text provenance: Primarily AI-generated text.* Most of the mathematical exposition was generated by AI systems through an extended process of human direction, discussion, and revision. Generative AI was also used substantially in the mathematical exploration underlying this manuscript. Igor Zelenko formulated the regularity targets, suggested an initial approach through weighted second variations, and directed an extended investigation of candidate constructions. His interventions included considering smooth nonhomogeneous structures, distinguishing rigidity from length minimality, requiring comparisons involving simultaneous changes in several regions, and questioning whether successive modifications could remain finite-dimensional.

ChatGPT (OpenAI, using Astra) generated explicit candidate constructions, proposed shortening competitors and modifications, developed proposed proof arguments, and produced initial drafts of the mathematical exposition. The twelve-dimensional candidate emerged through repeated requests to address unresolved cases and to modify unsuccessful constructions while preserving the comparisons already obtained. Thus the use of AI extended to the construction and mathematical reasoning, and was not limited to writing or editing. Claude (Anthropic) was subsequently used for additional AI-assisted review and suggestions for revision.

Bangjie Wang joined the project and, with ChatGPT assistance, reduced the ambient dimension from twelve to six by reorganizing the auxiliary coordinates and consolidating the integral constraints. This also simplified the length comparisons and removed the need for a separate cubic-moment estimate in the twelve-dimensional draft. The second author, Igor Zelenko, subsequently recognized the connection with Weierstrass excess and Hilbert invariant-integral comparisons in the classical calculus of variations. The first author, Bangjie Wang, further related these comparisons to smooth subsolutions of stationary Hamilton–Jacobi inequalities. With further AI assistance, these viewpoints were developed into the finite cell comparisons and the induction used in the present proof. In particular, the Hamilton–Jacobi formulation expresses several length comparisons through a common differential inequality, while the Hilbert formulation identifies the corresponding integrals fixed by the lifted endpoints. These developments substantially simplified several steps and, we hope, made the proof more accessible conceptually.

*Lean formalization and its scope.* The first author, Bangjie Wang, formalized Theorem 1 in the proof assistant Lean 4 (version 4.30.0, with Mathlib v4.30.0). The Lean formalization was developed with AI assistance from OpenAI's Codex. The sources, together with build instructions, are available at `https://zenodo.org/records/24450367`.

The package formalizes the main existence theorem and its proof route. This is not a claim that every sentence of the manuscript has been formally checked. The supplementary assertions on intrinsic nonanalyticity and lifting, the announced Hölder results, and all explanatory discussions of the single-cell model and Hilbert invariant integrals are outside the package's stated coverage. These supplementary assertions and explanatory discussions are not premises of the formalized main theorem.

*Human understanding: some parts.* The authors have checked and understood parts of this contribution. We are reasonably confident in the correctness of the construction and the proof presented here, but our detailed human verification of the manuscript remains in progress and requires further time. We are circulating this preliminary version to invite independent scrutiny. Given the significance of the proposed counterexample for the regularity problem, we believe that sharing the construction and its arguments at this stage may benefit the sub-Riemannian research community while human verification continues. We take responsibility for the content of the manuscript and for correcting any errors identified in the course of this process.

## 2 The curve and its horizontal equations

The example is a lift of a planar graph with increasingly narrow pulses (the graph pieces on the cells of Definition 6.1). We first give the form of the lift and its differential equations. The coefficient functions in these equations will be specified together in Section 6; the intervening sections explain what each coordinate is intended to accomplish.

Write the six coordinates as

$$(t, x, r, \xi, W, Z). \tag{2.1}$$

The variable $t$ is the clock and $x$ is the spatial coordinate. The reference graph $x = f(t)$ is zero for $t \le 0$ and in the gaps between disjoint positive intervals, called cells, which accumulate at zero. On each cell it makes a small excursion and returns to zero. Its amplitude is negligible compared with the distance of that cell from zero, but the slope at the center has a fixed positive size. Thus $f(t) = o(t)$, although $f'$ does not tend to zero. Figure 1 shows the graph and its unit velocity.

The four auxiliary coordinates obey

$$\begin{aligned} dr &= (-q_x(t,x) + e(t))\,dt, \\ d\xi &= -(r - \rho_-(t)x)\,dt + q(t,x)\,dx, \\ dW &= \left(\sum_n m_n Q_n(t,x) + \xi^6\right) dt, \\ dZ &= \left(\xi^{10} + \sum_n m_n \chi_n(t)(W - w_n)^2\right) dt. \end{aligned} \tag{2.2}$$

Here $q$ is a function of clock and position, $e$ is a clock correction, and $\rho_-$ is supported on the negative clock axis. Each $Q_n$ is an integral density supported on the $n$-th cell; $m_n > 0$ is its weight. The nonnegative function $\chi_n$ is supported in the gap immediately below that cell, and $w_n$ is a prescribed accumulated value on that gap. These descriptions fix the roles and arguments of the coefficients, not their values. The construction will arrange that the assembled coefficients are smooth.

The candidate has the form

$$\Gamma_a(t) = (t, f(t), r_*(t), 0, W_*(t), 0). \tag{2.3}$$

Thus $\xi$ and $Z$ remain zero on the reference; $r_*$ and $W_*$ are its other auxiliary coordinates. The positive amplitude parameter $a$ is small and fixed. A short segment with negative initial clock and positive terminal clock will be the minimizing arc.

### 2.1 Horizontal lifts and length

For $\mathbf{y} = (r, \xi, W, Z)$, a system prescribing the auxiliary velocities has the form

$$d\mathbf{y} = \mathbf{Q}(t, x, \mathbf{y})\,dt + \mathbf{P}(t, x, \mathbf{y})\,dx. \tag{2.4}$$

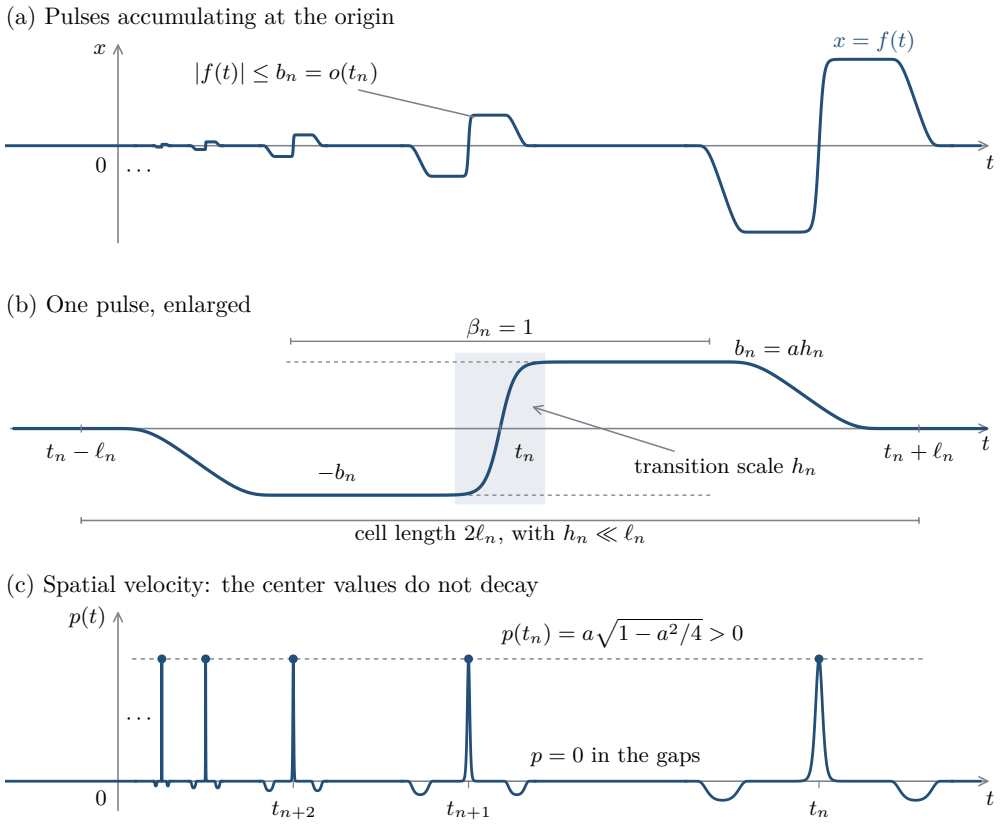


Figure 1: The reference projection and its spatial unit velocity (schematic). The cells accumulate at zero. Within a cell of width $2\ell_n$, a transition of width $h_n$ has amplitude of order $b_n = ah_n$, with fixed $a > 0$. The graph returns to the clock axis outside the transition. Heights tend to zero, while center velocities stay fixed and the velocity on each gap is $(1, 0)$. The sequences and profile are specified in Section 6.

It defines a rank-two distribution by the Pfaffian equations

$$dy^i - Q^i\,dt - P^i\,dx = 0, \qquad i = 1, \dots, 4,$$

or, equivalently, by the coordinate vector fields

$$X_1 = \partial_t + \sum_i Q^i \partial_{y^i}, \qquad X_2 = \partial_x + \sum_i P^i \partial_{y^i}.$$

A tangent vector is horizontal precisely when it is $u_t X_1 + u_x X_2$. Its planar projection is $u_t \partial_t + u_x \partial_x$. Declaring $X_1, X_2$ orthonormal therefore makes horizontal length exactly planar length:

$$L(\gamma) = \int \sqrt{\dot{t}^{\,2} + \dot{x}^{\,2}}\, ds. \tag{2.5}$$

The clock pauses when $\dot{t} = 0$ and reverses when $\dot{t} < 0$. During a pause, $x$ may still vary; integrals with respect to $dt$ retain the sign of $\dot{t}$. For (2.2), the auxiliary equations are solved successively in the order $r, \xi, W, Z$. Once their coefficients are smooth, a prescribed planar path and initial values have a unique local lift. A planar shortening is an admissible competitor only when that lift also reaches all four terminal auxiliary values. The coordinates change the endpoint constraints, while the metric continues to measure planar length.

# 3 A smooth transition and its Hamilton–Jacobi subsolution

We first construct one smooth transition with all four auxiliary coordinates present. Its minimality follows from a single function whose differential has horizontal norm at most one. The construction also gives a bracket-generating frame near the reference arc.

## 3.1 The transition and its horizontal lift

We determine the transition from a length comparison. First introduce one accumulated coordinate $w$ by $dw = V(x)\,dt$. Equal lifted endpoints fix this signed integral. Seek a smooth comparison function $S = t + \Psi(x) - \kappa w$ whose horizontal derivatives are a unit vector $(C, P)$. This requires

$$C = 1 - \kappa V, \qquad P = \Psi', \qquad C^2 + P^2 = 1.$$

The reference should follow that vector, so $f' = P(f)/C(f)$. For a graph on $[t_0, t_1]$, the augmented functional is

$$J_\kappa(x) = \int_{t_0}^{t_1} \left( \sqrt{1 + x'(t)^2} + \kappa V(x(t)) \right) dt.$$

We call $V$ the potential because it contributes the position-dependent term in this integrand. The multiplier $\kappa$ enters the comparison, not the equation $dw = V\,dt$; equal $w$-endpoints fix the added integral. To approach the levels $x = \pm a$ with zero slope, take a nonnegative potential vanishing at both levels. A smooth nonnegative polynomial has zeros of even order; the lowest-degree choice with these two zeros is a positive multiple of $(x^2 - a^2)^2$. Its double zeros make $P$ vanish linearly, giving the exponential tails needed for localization. Absorb the positive multiple into $\kappa$. Choosing $\kappa a^4 = a^2/2$ makes the central spatial unit velocity comparable to the small parameter $a$. Thus, for $0 < a \le 1/4$, set

$$V(x) = (x^2 - a^2)^2, \qquad \kappa = \frac{1}{2a^2}, \qquad C(x) = 1 - \kappa V(x), \qquad P(x) = \sqrt{1 - C(x)^2} \quad (-a < x < a). \tag{3.1}$$

Here $0 < C < 1$ and $P > 0$. Let $f$ solve

$$f'(t) = P(f(t))/C(f(t)), \qquad f(0) = 0.$$

Equivalently, $f$ is the inverse of

$$x \longmapsto \int_0^x \frac{C(y)}{P(y)}\,dy.$$

Since $V$ has a double zero at each of $\pm a$, $P(x) = \sqrt{2\kappa V(x) - \kappa^2 V(x)^2}$ vanishes linearly there. Thus $C/P$ has a positive simple-pole asymptotic at both ends. The integral is strictly increasing onto $\mathbb{R}$, so $f$ is smooth on $\mathbb{R}$ and approaches $\pm a$ as $t \to \pm\infty$.

Set $W_*(t) = \int_0^t V(f(u))\,du$. On $\mathbb{R} \times (-a, a) \times \mathbb{R}^4$, with coordinates $(t, x, r, \xi, W, Z)$, prescribe

$$\begin{aligned} dr &= -C'(x)\,dt, \\ d\xi &= C(x)\,dx - r\,dt, \\ dW &= (V(x) + \xi^6)\,dt, \\ dZ &= \left(\xi^{10} + (W - W_*(t))^2\right) dt. \end{aligned} \tag{3.2}$$

The even powers six and ten will be justified in Subsection 6.3 by the accuracy required when infinitely many transitions are combined. Their exact values are not needed to understand the

single-transition comparison. All coefficients are smooth. Declare the two fields

$$\begin{aligned} X_1 &= \partial_t - C'(x)\partial_r - r\partial_\xi + (V(x)+\xi^6)\partial_W + (\xi^{10} + (W - W_*(t))^2)\partial_Z, \\ X_2 &= \partial_x + C(x)\partial_\xi \end{aligned} \tag{3.3}$$

orthonormal. As in (2.5), horizontal length is planar length. The reference lift is

$$\Gamma_*(t) = (t, f(t), P(f(t)), 0, W_*(t), 0). \tag{3.4}$$

We call the whole planar graph $t \mapsto (t, f(t))$ the *standard transition*. Its compact segments are the smooth reference arcs used in this model; they do not yet include returns to the clock axis.

The four coordinates have distinct roles. The coordinate $W$ records the potential integral, with a nonnegative extra rate when $\xi \neq 0$. The coordinate $r$ records the reference spatial unit velocity. The equation for $\xi$ compares $C(x)\,dx$ with $r\,dt$; these agree along the reference. The coordinate $Z$ tests both $\xi$ and the discrepancy $W - W_*(t)$.

In particular, $r$ is not zero on the reference. If $R = r - P(f(t))$, then on a smooth graph parametrized by $t$,

$$R' = -(C'(x) - C'(f)), \qquad \xi' = C(x)x' - C(f)f' - R.$$

The vanishing reference quantities are $R$ and $\xi$. For another graph, requiring $\xi = 0$ determines $r = C(x)x'$ and hence imposes the differential equation

$$\frac{d}{dt}(C(x)x') = -C'(x).$$

Thus these coordinates constrain horizontal competitors as well as supplying bracket directions.

### 3.2 Bracket generation and unique minimality

The next proposition establishes both geometric and variational properties of the complete model. Competitors may pause or reverse their clock.

**Proposition 3.1.** *Every compact segment of $\Gamma_*$ is a smooth horizontal curve. On a neighborhood of that segment, the frame (3.3) is bracket-generating, and the segment uniquely minimizes length among horizontal curves in that neighborhood with the same ordered endpoints, up to nondecreasing reparametrization. Brackets of length at most 11 suffice along the reference.*

*Proof.* We prove horizontality, bracket generation, and minimality in turn.

*Horizontality.* Differentiating $C^2 + P^2 = 1$ gives $PP' = -CC'$, so

$$\frac{d}{dt}P(f(t)) = P'(f)\frac{P(f)}{C(f)} = -C'(f).$$

Also $C(f)f' = P(f)$. These identities prove the first two laws in (3.2); the last two follow from the definition of $W_*$. In arclength the reference planar velocity is $(C(f), P(f))$, since $C > 0$ and $C^2 + P^2 = 1$.

*Bracket generation.* Choose a primitive $B' = C$, and use $\zeta = \xi - B(x)$. In the following formulas, $\xi = \zeta + B(x)$ denotes the original coordinate expressed in the new variables. The fields become

$$\begin{aligned} Y_1 &= \partial_t - C'(x)\partial_r - r\partial_\zeta + (V(x)+\xi^6)\partial_W + (\xi^{10} + (W - W_*(t))^2)\partial_Z, \\ Y_2 &= \partial_x. \end{aligned}$$

All $x$-derivatives below hold $\zeta$ fixed. At a point where $\xi = 0$, the first $m-1$ derivatives of $\xi^m$ vanish and $\partial_x^m(\xi^m) = m!C(x)^m$: in the product of $m$ factors, the only surviving term differentiates each factor once.

Put $T = \mathrm{ad}_{Y_2}^3 Y_1$. Since $C^{(4)} = -24\kappa$ and $V^{(3)} = 24x$,

$$T = 24\kappa\,\partial_r + 24x\,\partial_W \quad \text{at } \xi = 0.$$

For the next bracket, we use the coefficients of $T$ on the whole neighborhood: its $t, x, \zeta$ components vanish and its $r$-component is the constant $24\kappa$. It follows directly that

$$[T, Y_1] = -24\kappa\,\partial_\zeta \pmod{\operatorname{span}\{\partial_W, \partial_Z\}}.$$

This calculation does not differentiate an identity restricted to $\xi = 0$. At such a point the higher spatial brackets give

$$\mathrm{ad}_{Y_2}^6 Y_1 = 6!C(x)^6\partial_W, \qquad \mathrm{ad}_{Y_2}^{10} Y_1 = 10!C(x)^{10}\partial_Z \pmod{\mathbb{R}\partial_W}.$$

The last two fields span the $W, Z$ directions. Subtracting those components from $T$ and $[T, Y_1]$ gives the $r, \zeta$ directions. Finally $Y_1, Y_2$ have independent $t, x$ projections. The resulting six fields are independent because $C > 0$ and $\kappa > 0$. Their bracket lengths are $1, 1, 4, 5, 7, 11$. Their determinant remains nonzero on a neighborhood of the compact reference segment.

*Minimality.* Let $\Psi' = P$ on $(-a, a)$, and set

$$S(t, x, r, \xi, W, Z) = t + \Psi(x) - \kappa W.$$

Evaluation on the orthonormal frame gives

$$X_1 S = C(x) - \kappa\xi^6, \qquad X_2 S = P(x).$$

Shrink the preceding neighborhood so that $\kappa\xi^6 < 2C(x)$. Then

$$(X_1 S)^2 + (X_2 S)^2 = 1 - \kappa\xi^6(2C(x) - \kappa\xi^6) \le 1, \tag{3.5}$$

with equality precisely when $\xi = 0$. For a horizontal curve with control $(u_t, u_x)$, Cauchy–Schwarz yields

$$\frac{dS}{ds} = (X_1 S)u_t + (X_2 S)u_x \le \sqrt{u_t^2 + u_x^2}.$$

Integrating proves that its length is at least the difference of the endpoint values of $S$. Along the reference, $\xi = 0$ and the unit control is $(C, P)$, so equality holds everywhere.

If a competitor has the same length, parametrize it by arclength. Equality in the integrated inequality implies equality almost everywhere in both the norm bound and Cauchy–Schwarz. Consequently $\xi = 0$ and $(u_t, u_x) = (C(x), P(x))$ almost everywhere. On a sufficiently small neighborhood of the compact reference segment, $C$ is bounded below by a positive constant. The clock therefore has a Lipschitz inverse, and $dx/dt = P(x)/C(x)$. Uniqueness for this smooth scalar ODE identifies the planar reference from the common initial point. The successive equations for $r, \xi, W, Z$ then identify its lift. In an arbitrary parameter, the only remaining freedom is a nondecreasing reparametrization. □

For the sub-Riemannian Hamiltonian

$$\mathcal{H}(\lambda) = \tfrac{1}{2}(\lambda(X_1)^2 + \lambda(X_2)^2), \qquad \lambda \in T^*U,$$

where $U$ is the comparison neighborhood, (3.5) is the Hamilton–Jacobi subsolution inequality $\mathcal{H}(dS) \le 1/2$, sharp on the reference. The exact differential $dS$ has an integral fixed by the endpoints: this is its Hilbert invariant-integral interpretation [11, §23]. The nonnegative difference between length and this differential proves minimality. The argument uses the $W$-endpoint but not the $Z$-endpoint. The two powers of $\xi$ nevertheless supply independent bracket directions. When several transitions are assembled, the separate integral constraints supplied by $Z$ will enter the length proof.

For later localization, the underlying planar identity is also useful. For an arclength-parametrized planar curve with unit velocity $u$,

$$1 + \kappa V(x)t' = t' + P(x)x' + \tfrac{1}{2}|u - (C(x), P(x))|^2.$$

Indeed $1 - u \cdot (C, P) = |u - (C, P)|^2/2$ and $C = 1 - \kappa V$. Integrating $P\,dx = d\Psi$ and subtracting the reference gives, for the same ordered planar endpoints,

$$L - L_* + \kappa \left( \int V(x)\,dt - \int V(f)\,dt \right) = \frac{1}{2} \int |u - (C(x), P(x))|^2\,ds. \tag{3.6}$$

The clock integrals are signed, so this identity includes reversing clocks. It is the local identity used on the cores of the assembled pulses.

# 4 From a transition to accumulating pulses

A compact transition gives a smooth minimizer. To obtain a curve whose velocity oscillates near zero, we place progressively smaller transitions on disjoint cells accumulating there, while keeping their central slopes of fixed size. The reference must return to the clock axis between cells. These return portions and the accumulation point require changes to the single-cell system.

## 4.1 Returning to the clock axis

On the central plateau, where a pulse agrees with a rescaled standard transition ((6.9)), we retain the autonomous comparison field and its potential identity (3.6). On a return portion the graph no longer solves $f' = P(f)/C(f)$. We therefore cut off the potential and correct its first variation. On a single cell let $f$ be the smooth reference pulse, $p = f'/\sqrt{1 + f'^2}$ its spatial unit velocity, and $\Phi(t, x)$ a localized potential. For a smooth variation $f + \epsilon y$ fixing the cell endpoints,

$$\frac{d}{d\epsilon}\Big|_0 \int \sqrt{1 + (f' + \epsilon y')^2}\,dt = \int py'\,dt = -\int p'y\,dt.$$

Thus the augmented length is stationary at $f$ if $Q_x(t, f) = \kappa^{-1}p'$. This gives the form

$$Q(t, x) = \Phi(t, x) + (\kappa^{-1}p'(t) - \Phi_x(t, f(t)))(x - f(t)) + K(t)(x - f(t))^2.$$

The linear correction is determined by stationarity. The quadratic term changes neither the value nor the first derivative on the reference; its coefficient will allow the autonomous comparison to be joined to a comparison on the return portions. In Section 12 we construct local functions $\Psi$ satisfying

$$(1 + \Psi_t - \kappa Q)^2 + \Psi_x^2 \le 1,$$

with equality in the reference direction. A smooth localization gives such a function on the whole cell: the quadratic term supplies the inward margin needed in its differential.

### 4.2 Preserving the reference phase equations

The same return also changes the reference $r$-velocity. We keep the form of the single-cell equations and add a clock correction. For a smooth pulse $f$ and coefficient $q(t,x)$, retain

$$r_*(t) = q(t, f(t))f'(t), \qquad t \neq 0, \tag{4.1}$$

and correct the $r$-equation by a function of clock alone:

$$e(t) = r_*'(t) + q_x(t, f(t)). \tag{4.2}$$

The complete pair of laws is

$$dr = (-q_x + e)\,dt, \qquad d\xi = -(r - \rho_-(t)x)\,dt + q(t,x)\,dx. \tag{4.3}$$

The additional smooth function $\rho_-$, supported on $t \leq 0$, will be flat at zero and nonzero for negative clocks. Since the reference has $f = 0$ there, this addition does not affect the cancellation. Its role in intrinsic nonanalyticity is separate from the length proof.

On a positive-clock interval, where $\rho_- = 0$, consider a smooth competitor graph and write $R = r - r_*(t)$. Subtracting the reference equations gives

$$\begin{aligned} R' &= -\big(q_x(t,x) - q_x(t, f(t))\big), \\ \xi' &= q(t,x)x' - q(t, f(t))f'(t) - R. \end{aligned} \tag{4.4}$$

The first equation records the difference between the evolution of $r$ on the two paths. The second compares their weighted spatial velocities and subtracts that accumulated difference. Both right-hand sides vanish on $x = f$, $R = 0$. For a competitor, however, even the condition $\xi = 0$ is restrictive: it determines $r = q(t,x)x'$, whose derivative must still satisfy the $r$-equation.

The reference compatibility persists under this correction, while the core cancellation persists under a constant rescaling of $q$.

**Proposition 4.1.** *Let $f$ be a smooth graph on an interval, let $q(t,x)$ be smooth, and suppose $\rho_-(t)f(t) = 0$. Define $r_*$ and $e$ by (4.1)–(4.2). Then $(t, f(t), r_*(t), 0)$ satisfies (4.3). On any subinterval where $\rho_- = 0$, a smooth graph $x(t)$ has a lift satisfying these laws with $\xi \equiv 0$ if and only if*

$$\frac{d}{dt}\big(q(t,x(t))x'(t)\big) = -q_x(t,x(t)) + e(t); \tag{4.5}$$

*its $r$-coordinate is necessarily $q(t,x(t))x'(t)$. If, on this interval, smooth functions $C, P$ satisfy*

$$C^2 + P^2 = 1, \qquad C > 0, \qquad f' = P(f)/C(f), \qquad q(t,x) = \omega C(x), \quad \omega > 0 \text{ constant},$$

*then $r_* = \omega P(f)$ and $e = 0$.*

*Proof.* By definition, $r_*' = -q_x(t,f) + e$. Substituting the reference into the second equation gives $-r_* + \rho_- f + q(t,f)f' = 0$. When $\rho_- = 0$, the equation $\xi' = 0$ is exactly $r = q(t,x)x'$. Substitution into the $r$-equation gives (4.5). Conversely, a solution of that equation, together with $r = q(t,x)x'$ and $\xi = 0$, satisfies both laws. For $q = \omega C$, one has $r_* = \omega P(f)$. The identity $PP' = -CC'$ used in Proposition 3.1 gives $r_*' = -\omega C'(f) = -q_x(t,f)$, hence $e = 0$. □

The choice $q = \omega C$ also determines a useful extension beyond the transition. For the quartic potential with preferred levels $\pm b$, write

$$C(x) = 1 - \kappa(x^2 - b^2)^2, \qquad A^2 = (2\kappa)^{-1}.$$

Choosing $\omega = A^2$ gives $q = A^2 - \frac{1}{2}(x^2 - b^2)^2$. To assemble pulses, we replace $A, b$ by smooth clock-dependent amplitudes $A_*(t), b_*(t)$, constant on each central plateau and zero in the gaps. This leads to

$$q(t,x) = A_*(t)^2 - \tfrac{1}{2}(b_*(t)^2 - x^2)^2 = -\tfrac{1}{2}x^4 + b_*(t)^2x^2 + A_*(t)^2 - \tfrac{1}{2}b_*(t)^4.$$

Section 6 specifies these amplitudes. On each plateau, the preceding proposition gives $e = 0$; on the return portions, $e$ restores the reference equation. The coefficient $q$ uses the smooth amplitudes rather than the oscillating slope $f'$.

In the gaps, this extension retains $q_0(x) = -x^4/2$. Its derivative contributes $2x^3\partial_r$ to the clock field. Three brackets with the spatial field will produce the $r$-direction, and the term $-r\partial_\xi$ will then produce the $\xi$-direction. Moreover, if $A_*, b_*$ are flat at zero, the displayed expansion shows that $q - q_0$ is flat there. The smoothness estimates in Section 8 establish this flatness and the corresponding bounds for the other coefficients, so that these bracket directions persist for the assembled construction.

### 4.3 Why the observations must be localized

On cell $I_n$, let $Q_n$ be the corrected density and $m_n > 0$ its weight. Recording $\sum_n m_n Q_n$ in $W$ prescribes only the total weighted integral at the terminal point. The local length identities, however, use the individual cell integrals with their own multipliers $\kappa_n$.

In the single-cell model, $W_*(t)$ is smooth and can appear directly in the $Z$-equation. Smoothness of the assembled field does not give smoothness of its integral along the oscillating reference. For example, let the transition width be $h_n$ and its amplitude be $b_n = ah_n$. With the weights and widths chosen in (6.1), the reference rate on a central plateau is

$$W_*'(t) = m_n a^4 h_n^4 H_a((t - t_n)/h_n), \qquad H_a(\tau) = (1 - F_a(\tau)^2)^2,$$

where $F_a(\tau) = f(\tau)/a$ for the transition of Section 3; Section 6 gives its rescaled form. The smooth function $H_a$ is positive and tends to zero at both ends, so it cannot be a polynomial; in particular, $H_a^{(5)}$ is not identically zero. Fix $\tau_0$ with $H_a^{(5)}(\tau_0) \neq 0$. For large $n$, the point $t_n + h_n\tau_0$ lies in the plateau, and

$$W_*^{(6)}(t_n + h_n\tau_0) = m_n a^4 h_n^{-1} H_a^{(5)}(\tau_0).$$

The scales (6.1) give $m_n/h_n \to \infty$, so these derivatives are unbounded. Thus this choice does not permit the full function $W_*(t)$ as a smooth frame coefficient.

In each gap, by contrast, the reference integral is constant. We test against that constant only within the gap. This also has an analytic advantage: no cell density is active during a test, so the discrepancy changes only through the additional term $\xi^6$. The next section gives the resulting observation system.

## 5 Recovering the separate cell integrals

We now replace the full-time test in (3.2) by tests supported in the gaps. The states $r, \xi$ and their corrected equations (4.3) are retained.

Let $I_n$ be disjoint open clock intervals, ordered so that $I_{n+1}$ lies below $I_n$, and let $G_n$ be the intervening gap. Let $Q_n(t,x)$ be continuous densities supported in $I_n$, $m_n > 0$, and let $\chi_n$ be nonzero nonnegative continuous functions compactly supported in $G_n$. Define

$$W_*(t) = \int_0^t \sum_n m_n Q_n(u, f(u))\, du, \qquad w_n = W_*|_{G_n}.$$

Assume these sums and integrals are well defined and the rates are continuous along the paths under consideration. The explicit construction below gives smooth frame coefficients. The observation equations are

$$\begin{aligned} dW &= \left(\sum_n m_n Q_n + \xi^d\right) dt, \\ dZ &= \left(\xi^k + \sum_n m_n \chi_n (W - w_n)^2\right) dt, \qquad d = 6, \quad k = 10. \end{aligned} \tag{5.1}$$

We retain the letters $d, k$ in the later estimates to distinguish the two powers. On the reference, $\xi = Z = 0$ and $W = W_*$. Only the gap constants $w_n$, rather than the whole function $W_*$, occur in the coefficients.

For example, suppose three successive cells contribute weighted integrals $2, 3, 1$ along the reference. Their successive accumulated values are $2, 5, 6$. Contributions $1, 4, 1$ have the same total but give the intermediate values $1, 5, 6$. At the first intervening test, the second path has a nonzero squared discrepancy. Restoring the correct accumulated value at the next test cannot subtract that earlier contribution to $Z$ when the clock is increasing. These numbers illustrate the endpoint constraints; they do not assert the existence of a planar path realizing any prescribed list of cell integrals.

The nonnegative rate of $Z$ separates these tests when the clock is increasing.

**Proposition 5.1.** *An absolutely continuous path satisfying (5.1), with strictly increasing clock and zero $Z$-endpoints, has $\xi = 0$ everywhere and $W = w_n$ wherever $\chi_n > 0$. If it crosses both adjacent gap tests of $I_n$ completely, then*

$$\int_{I_n} Q_n(t, x(t))\, dt = \int_{I_n} Q_n(t, f(t))\, dt.$$

*Here $x(t)$ is the continuous graph obtained by inverting the clock.*

*Proof.* The continuous rate of $Z$ is nonnegative and has zero integral against $dt$. Every nonempty open parameter interval has positive $dt$-measure because the clock is strictly increasing. If any summand were positive at a point, continuity would give a positive integral on a surrounding interval. Thus every summand vanishes: $\xi = 0$ and $W = w_n$ on the $n$-th test.

On a gap the cell densities vanish, and $\xi = 0$, so $W$ is constant throughout that gap. Its values on the two sides of $I_n$ are therefore $w_n$ and $w_{n-1}$. Integrating the $W$-equation across that cell gives

$$m_n \int_{I_n} Q_n(t, x(t))\, dt = w_{n-1} - w_n = m_n \int_{I_n} Q_n(t, f(t))\, dt.$$

Division by $m_n > 0$ proves the assertion. □

Each cell integral equals its own reference value; the different cell integrals need not equal one another. The state $W$ retains the accumulated integral, which the current planar position alone does not determine. The state $Z$ tests that retained value. On smooth portions with positive clock, its vanishing also imposes the phase equation (4.5).

For a reversing clock the same law reads

$$\dot{Z} = \left(\xi^{10} + \sum_n m_n \chi_n(t)(W - w_n)^2\right) \dot{t}.$$

Backward visits can cancel forward contributions. The later length proof measures these visits by the fixed clock defect (9.1) and recovers the cell integrals with higher-order errors. The gap support is used at that step: there

$$\frac{d}{ds}(W - w_n) = \xi^6 \dot{t},$$

without a contribution from the unknown density $Q_n(t,x)$. Section 10 turns this identity into the quantitative endpoint estimate.

The bracket calculation at the accumulation point also differs from the single-cell calculation. There the coefficient $q$ tends to $-x^4/2$, which vanishes at $x=0$; the direct spatial derivatives used in Proposition 3.1 no longer produce $W, Z$ at the same orders. Section 8 computes the brackets of the limiting frame after proving smoothness.

# 6 The complete construction

We now specify the coefficients of (2.2) and the reference graph. The formulas depend on a small positive parameter $a$, common to all cells and chosen in Section 13. Smoothness at zero and minimality will be proved in the following sections; all the functions and endpoints are defined here.

## 6.1 Scales and cells

Take $0 < a \le 1/4$. The three clock scales have different jobs. The centers $t_n$ and cell widths $\ell_n$ locate separated pulses and leave gaps for the tests. The transition width $h_n$ determines the excess length of one pulse. Scaling both clock and space by $h_n$ preserves the slopes of the model, so its spatial amplitude must be $b_n = ah_n$. The quartic potential then scales by $h_n^4$, and its multiplier scales inversely:

$$\kappa_n = (2a^2h_n^4)^{-1}, \qquad A_n = ah_n^2.$$

This is why the two amplitudes $b_n$ and $A_n$ have different powers of $h_n$; the exact scaling identity is (8.4).

The weights $m_n$ must make the observation coefficients smooth at zero, but small weights amplify the error when a recorded integral is recovered. We resolve this conflict by making the transition width much smaller still. We make the following explicit choice.

For integer $n \ge n_0$, set

$$t_n = 2^{-n}, \qquad \ell_n = t_n/16, \qquad m_n = e^{-1/t_n^2}, \qquad h_n = e^{-e^{n^2}}. \tag{6.1}$$

The ratio $\ell_n/t_n = 1/16$ is only a geometric convenience: successive centers have ratio $1/2$, so this leaves gaps of size comparable to $t_n$. The two decay rates serve separate analytic purposes:

$$\log(1/m_n) = 4^n, \qquad \log(1/h_n) = e^{n^2}, \qquad \frac{\log(1/m_n)}{\log(1/h_n)} \longrightarrow 0.$$

Consequently $m_n$ decays faster than every fixed power of the cell width, while the inverse observation weights grow more slowly than any fixed inverse power of $h_n$. The quantitative version is (10.10). These rates are sufficient choices, not optimized ones. Smoothness does not follow from the weights alone: uncancelled derivatives on the much narrower scale $h_n$ would be too large. Lemma 8.8 proves exact cancellation on the cores, and Lemma 8.10 uses exponential profile tails off the cores.

Choose $n_0$ large enough that $\ell_n > 4h_n$ for $n \ge n_0$. All sums below start at $n_0$.

**Definition 6.1** (Cells, pulses, and gaps)**.** The cells and the gaps on their sides facing the origin are

$$I_n = (t_n - \ell_n, t_n + \ell_n), \qquad G_n = (t_{n+1} + \ell_{n+1}, t_n - \ell_n). \tag{6.2}$$

The graph restricted to $I_n$ is its $n$-th planar pulse; its horizontal lift restricted to $I_n$ is the lifted pulse.

For these scales,

$$G_n = \left(\frac{17}{32}t_n, \frac{15}{16}t_n\right), \qquad |G_n| = \frac{13}{32}t_n. \tag{6.3}$$

### 6.2 The localized profile and its density

The fixed-scale transition is $\tau \mapsto (\tau, aF_a(\tau))$. Its normalized scalar profile solves

$$F_a'(\tau) = \frac{v_a(F_a(\tau))}{c_a(F_a(\tau))}, \qquad F_a(0) = 0, \tag{6.4}$$

where

$$c_a(u) = 1 - \tfrac{1}{2}a^2(1-u^2)^2, \qquad v_a(u) = (1-u^2)\sqrt{1 - \tfrac{1}{4}a^2(1-u^2)^2}. \tag{6.5}$$

Separating variables in (6.4), $F_a$ is the inverse of $u \mapsto \int_0^u c_a(v)/v_a(v)\,dv$. This map is strictly increasing from $(-1,1)$ onto $\mathbb{R}$. The endpoint behavior was proved in Section 3; the uniform tail estimates are in Lemma 8.4.

Choose a smooth even function $0 \le \theta_\beta \le 1$, compactly supported in $(-1,1)$, equal to one on $[-1/2, 1/2]$, and nonincreasing on $[0,\infty)$. Put $\beta = \theta_\beta^4$. This power ensures $|\beta'| + |\beta''| \le C\sqrt{\beta}$: each term in those derivatives contains at least $\theta_\beta^2$. With $\beta = \theta_\beta^N$, the second derivative requires $N - 2 \ge N/2$, and four is the smallest integer meeting this bound. It will control the linear correction in Lemma 11.1 and the arclength peak in Lemma 11.3. Define

$$\eta(u) = \beta(4u), \qquad \vartheta(u) = \beta(u)(1-\eta(u)) + |\eta'(u)|. \tag{6.6}$$

The comparison cutoff $\eta$ switches off inside the plateau of the pulse cutoff $\beta$. Hence the uncut transition identities still hold wherever the comparison is being switched. The absolute value is smooth because $\eta$ is monotone on each side of zero and constant near zero. Set

$$F_{a,n}(t) = F_a((t-t_n)/h_n), \qquad \beta_n(t) = \beta((t-t_n)/\ell_n), \tag{6.7}$$

$$\eta_n(t) = \eta((t-t_n)/\ell_n), \qquad \vartheta_n(t) = \beta_n(t)(1-\eta_n(t)) + \ell_n|\eta_n'(t)|. \tag{6.8}$$

The reference graph is $f = \sum_{n \ge n_0} f_n$, extended by zero on the gaps and on $t \le 0$, where

$$f_n(t) = b_n \beta_n(t) F_{a,n}(t). \tag{6.9}$$

On $|t - t_n| \le \ell_n/2$ this is the scaled transition; near the cell endpoints it returns smoothly to zero. For fixed $R > 0$, a *transition window* means the interval

$$[t_n - Rh_n, t_n + Rh_n]. \tag{6.10}$$

Its scale is $h_n$, whereas the return and cutoff scale is $\ell_n$. The fixed ratio $b_n/h_n = a$ preserves the central slope; the ratio $b_n/\ell_n \to 0$ makes the return slope vanish. For $t \ne 0$, write its unit velocity as

$$\mathbf{h}_*(t) = (c(t), p(t)) = \frac{(1, f'(t))}{\sqrt{1 + f'(t)^2}}, \qquad e_t = (1,0). \tag{6.11}$$

and set $\mathbf{h}_*(0) = e_t$. Let $p_n = p|_{I_n}$.

The potential, multiplier, and unit comparison field on a cell are

$$A_n = ah_n^2, \qquad V_n(x) = (x^2 - b_n^2)^2, \qquad \kappa_n = \frac{1}{2A_n^2}. \tag{6.12}$$

$$C_n(x) = c_a(x/b_n), \qquad P_n(x) = a v_a(x/b_n). \tag{6.13}$$

Write $\mathbf{v}_n = (C_n, P_n)$. The formulas for $c_a, v_a$ are continued to larger spatial intervals where the square root is real. The signed factor $1 - u^2$ in $v_a$ gives a smooth continuation across $u = \pm 1$. The autonomous comparison is used on the central plateau, on bounded rescaled spatial bands.

Localize the potential and choose its quadratic correction by

$$\Phi_n(t,x) = \beta_n(t)\big(x^2 - b_n^2\beta_n(t)^2\big)^2. \tag{6.14}$$

The moving wells $\pm b_n\beta_n$ in $\Phi_n$ follow the slow return to zero. Away from the narrow transition, $f_n$ is exponentially close to one of these wells, so the reference potential remains small. The outer factor $\beta_n$ also makes the density vanish off the cell.

To choose the quadratic coefficient, write it provisionally as $K_n = c_K b_n^2 \vartheta_n$. For $y = x - f_n(t)$, the displacement remainder in the subsolution calculation is

$$\mathcal{R}_n = (1-\eta_n)\big[\Phi_n(t,x) - \Phi_n(t,f_n) - \Phi_{n,x}(t,f_n)y\big] + c_K b_n^2\vartheta_n y^2.$$

The quartic Taylor remainder has a negative part of size at most $2b_n^2\beta_n(1-\eta_n)(x-f_n)^2$. The weight $\vartheta_n$ therefore contains $\beta_n(1-\eta_n)$. Differentiating the comparison cutoff produces a second error, so it also contains $\ell_n|\eta_n'|$. The exact expansion in (12.6) gives

$$\mathcal{R}_n \geq (c_K - 2)b_n^2\vartheta_n(x-f_n)^2.$$

Any fixed $c_K > 2$ leaves an inward margin; taking it very large would worsen the upper bound needed to stay inside the unit ball. We choose the moderate value $c_K = 4$:

$$K_n(t) = 4b_n^2\vartheta_n(t). \tag{6.15}$$

The integral density is

$$\begin{aligned} Q_n(t,x) &= \Phi_n(t,x) + \big(\kappa_n^{-1}p_n'(t) - \partial_x\Phi_n(t,f(t))\big)y + K_n(t)y^2, \\ y &= x - f(t). \end{aligned} \tag{6.16}$$

Here $\kappa_n^{-1} = 2A_n^2$. The density and the pulse coefficients are extended by zero off $I_n$. The linear term is the stationarity correction derived in Subsection 4.1; the quadratic term vanishes near the transition center and supplies the inward correction in Section 12.

### 6.3 Gap tests, observation powers, and accumulated values

Choose a nonzero smooth function $0 \leq \theta \leq 1$ compactly supported in $(3/5, 4/5)$, and put $\chi = \theta^{10}$. Define the tests and their derivative bound by

$$|\chi'| \leq C\chi^{9/10}, \qquad \chi_n(t) = \chi(t/t_n). \tag{6.17}$$

The exponent ten matches $k = 10$ in the rate of $Z$: the bound $|\chi'| \leq C\chi^{1-1/k}$ prevents derivatives at a test edge from overwhelming the observation. For $\chi = \theta^N$ it follows from $N - 1 \geq N(1-1/k)$, or $N \geq k$. We use the smallest such power. The support $(3/5, 4/5)$ lies strictly inside the normalized gap $(17/32, 15/16)$; the particular fractions simply leave room on both sides. Set

$$M_n = \int_{\mathbb{R}} \chi_n(t)\,dt > 0, \qquad W_*(t) = \int_0^t \sum_n m_n Q_n(u, f(u))\,du. \tag{6.18}$$

The integral converges: on the reference the correction terms vanish, and

$$0 \leq Q_n(t, f(t)) = b_n^4\beta_n(t)^5(1 - F_{a,n}(t)^2)^2 \leq b_n^4, \qquad \sum_n m_n b_n^4 \ell_n < \infty.$$

The primitive is constant on $G_n$; denote that constant by $w_n$. Explicitly,

$$w_n = W_*(7t_n/10), \qquad M_n = c_\chi t_n, \qquad c_\chi = \int_{\mathbb{R}} \chi(u)\,du > 0. \tag{6.19}$$

Only the constants $w_n$, rather than the function $W_*$, enter the frame coefficients.

**Why the observation powers are six and ten.** The powers must do two jobs: separate bracket directions and make the endpoint errors smaller than a cell contribution. Temporarily write the two even powers as $d < k$. If $\mathcal{E}$ is the nonnegative rate of $Z$, differentiating a gap square produces a term bounded by $C\mathcal{E}^{1/2}|\xi|^d$. Since $|\xi|^k \le \mathcal{E}$, the derivative estimate used in Lemma 10.1 is valid when

$$\tfrac{1}{2} + d/k \ge 1 - 1/k, \qquad \text{equivalently} \qquad k \le 2d + 2.$$

The gap discrepancy then contributes an error of order $\mathfrak{B}^{(k+1)/2}$. The phase term has an unfavorable sign only during backward motion, contributing order $\mathfrak{B}^{d+1}$. Thus the relevant exponent is $\rho = \min\{d+1, (k+1)/2\}$; see Proposition 10.2 for these estimates.

A reference cell integral has scale $b_n^4 h_n = a^4 h_n^5$, whereas the old clock-defect bound has scale $a^2 h_n$. If the observation loss is at most $h_n^{-\varepsilon}$, its error relative to that integral has order

$$\frac{h_n^{-\varepsilon}(a^2 h_n)^\rho}{a^4 h_n^5} = a^{2\rho-4} h_n^{\rho-5-\varepsilon}.$$

The same exponent appears after summing the weighted errors in the length comparison. We therefore need $\rho > 5$; the scales (6.1) permit any fixed small $\varepsilon > 0$. The smallest even pair satisfying these requirements is

$$d = 6, \qquad k = 10, \qquad \rho = 11/2. \tag{6.20}$$

Taking $\varepsilon = 1/4$ leaves a positive margin of $1/4$ in the exponent of $h_n$. This explains the choices used in the frame; it asserts no optimality beyond these estimates.

### 6.4 The phase coefficients and the frame

The core identity in Proposition 4.1 suggests $q = A_n^2 C_n$ on a pulse plateau. To extend it across the return portions, define

$$b_*(t) = \sum_n b_n \beta_n(t), \qquad A_*(t) = \sum_n A_n \beta_n(t), \tag{6.21}$$

and

$$q(t,x) = A_*(t)^2 - \tfrac{1}{2}\big(b_*(t)^2 - x^2\big)^2, \qquad q_0(x) = -x^4/2. \tag{6.22}$$

Set $r_* = q(t,f)f'$ and $e = r_*' + q_x(t,f)$ for $t \ne 0$, as in (4.1)–(4.2), and assign both value zero at zero. Their regularity at zero is proved in Section 8. Finally, take

$$\rho_-(t) = \begin{cases} e^{-1/t^2}, & t < 0, \\ 0, & t \ge 0. \end{cases} \tag{6.23}$$

The completed frame is

$$\begin{aligned} X_1 &= \partial_t + (-q_x(t,x) + e(t))\partial_r - (r - \rho_-(t)x)\partial_\xi \\ &\quad + \left(\sum_n m_n Q_n(t,x) + \xi^6\right)\partial_W \\ &\quad + \left(\xi^{10} + \sum_n m_n \chi_n(t)(W - w_n)^2\right)\partial_Z, \\ X_2 &= \partial_x + q(t,x)\partial_\xi. \end{aligned} \tag{6.24}$$

Here $q, e, \rho_-$ are defined in (6.22), (4.2), and (6.23); $m_n, Q_n, \chi_n, w_n$ are defined in (6.1), (6.16), (6.17), and (6.19). Let $\mathcal{D}_a = \operatorname{span}\{X_1, X_2\}$, and let $g_a$ make these fields orthonormal. Their projections to the plane are $\partial_t, \partial_x$, so length is given by (2.5).

### 6.5 The reference and its endpoints

All functions in the reference are now specified:

$$\begin{aligned} \Gamma_a(t) &= (t, f(t), r_*(t), 0, W_*(t), 0), \\ s(t) &= \int_0^t \sqrt{1 + f'(\tau)^2}\, d\tau, \qquad \gamma(s(t)) = \Gamma_a(t). \end{aligned} \tag{6.25}$$

The graph $f$, phase coordinate $r_*$, and reference integral $W_*$ are specified by (6.9), (4.1), and (6.18), respectively. Choose $T_j = 7t_j/4$, and restrict to $-t_j \le t \le T_j$, with $j$ sufficiently large. The terminal clock lies in $G_{j-1}$, above its entire test support and below $I_{j-1}$. Its distance from the latter is $t_j/8$. A competitor is an absolutely continuous solution of (4.3), (5.1) with

$$\eta(0) = \Gamma_a(-t_j), \qquad \eta(T) = \Gamma_a(T_j), \tag{6.26}$$

in an arbitrary parameter, of length computed by (2.5). Its clock may pause or reverse. For sufficiently small fixed $a$ and sufficiently large $j$, we will prove that every such competitor of no greater length is a reparametrization of the reference.

## 7 Length minimization with ODE endpoint constraints

For the frame and reference defined in Section 6, we prove the following endpoint-constrained length statement.

**Proposition 7.1.** *There exists $a_0 > 0$ such that, for every fixed $0 < a \le a_0$, there is $j_0(a)$ with the following property. For every $j \ge j_0(a)$, the reference $\Gamma_a|_{[-t_j, T_j]}$ uniquely minimizes length among horizontal curves with the same endpoints, up to nondecreasing reparametrization. Every subarc has the same uniqueness property.*

We first establish the smoothness and geometric properties of the frame in Section 8. The proof of Proposition 7.1 then occupies Sections 9–13.

### 7.1 The endpoint problem

The terminal clock $T_j = 7t_j/4$ lies above the test in $G_{j-1}$, which ends before $8t_j/5$, and below the next cell $I_{j-1}$, which begins at $15t_j/8$. Hence

$$T_j \asymp t_j, \qquad \operatorname{dist}(T_j, I_{j-1}) = t_j/8. \tag{7.1}$$

A competitor that visits this larger cell and returns to the terminal clock must spend at least $t_j/8$ in backward clock variation. Lemma 9.1 will exclude such a visit using the reference pulse energy.

Figure 2 shows the kinds of planar modification which remain to be controlled. The statements concern horizontal competitors with all the prescribed auxiliary endpoints, not arbitrary planar shortcuts.

The coordinate laws have already been motivated for increasing clocks. For general clocks, Section 10 recovers each integral with an error. Section 11 first uses that information to confine the competitor in a region where the comparison field is defined. The length identity in Section 12 then bounds the clock defect by the next reference tail. Iterating this argument in Section 13 identifies the reference.

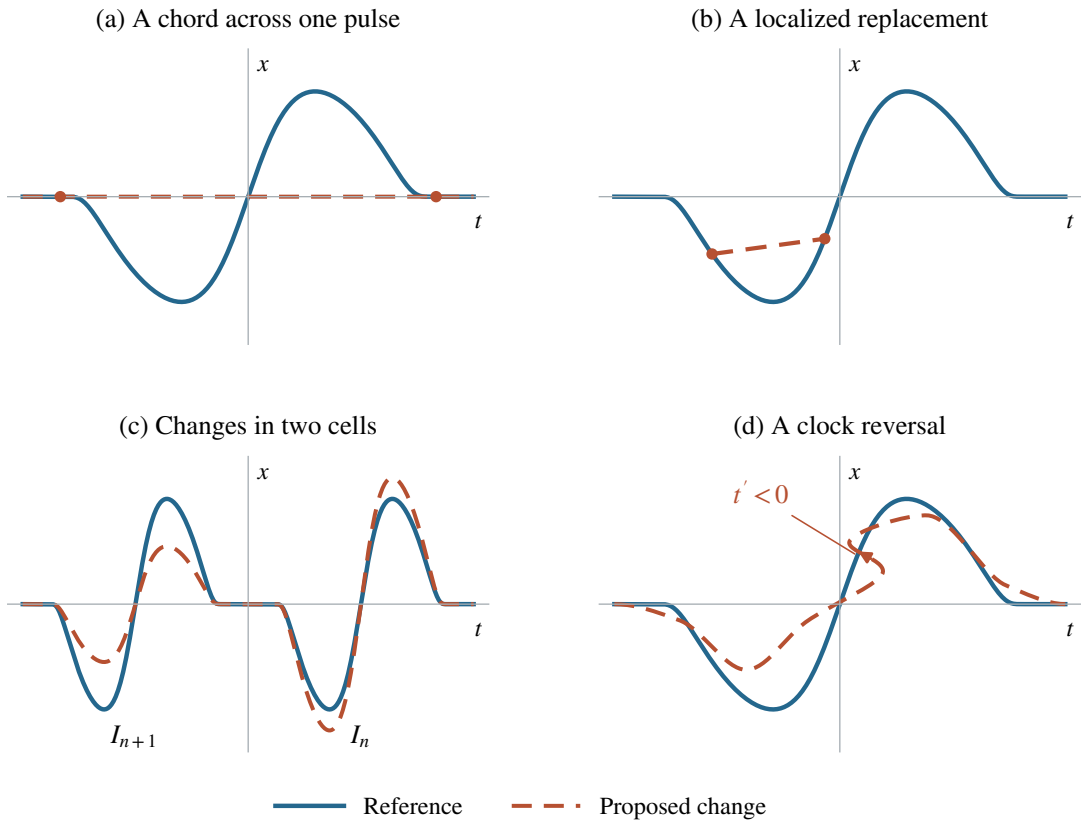


Figure 2: Schematic planar modifications that the endpoint constraints and length estimates must control. The solid curve is the reference; the dashed curve is a proposed replacement. (a) Replacing a whole pulse by a chord. (b) Replacing part of a pulse by a chord. (c) Modifying two cells simultaneously, with possible compensation in a recorded integral. (d) Reversing the clock, indicated by the leftward arrow. The drawings make no claim that the modified paths satisfy all auxiliary endpoint constraints, or that every depicted modification decreases length. No profile is prescribed by these schematic drawings.

# 8 Smoothness, brackets, and velocity limits

We prove the geometric assertions for the explicit frame (6.24) and reference (6.25).

**Proposition 8.1.** *For $0 < a \le 1/4$, the fields (6.24) define a smooth, bracket-generating rank-two sub-Riemannian structure near the origin. The reference is horizontal and differentiable at zero, with arclength derivative $X_1(0)$, but its arclength velocity has no continuous representative near zero. On every interval crossing zero it is a strictly abnormal extremal trajectory.*

## 8.1 Estimates for the rescaled transition

The profile in (6.4) is the normalized form of the transition in Section 3:

$$C(au) = c_a(u), \qquad P(au) = a v_a(u), \qquad f(\tau) = a F_a(\tau).$$

We now establish the uniform estimates needed when this profile is rescaled and cut off.

The inverse-integral definition of $F_a$ in Section 6 gives its global existence, oddness, and limits $\pm 1$. Thus the standard transition is the whole graph $\tau \mapsto (\tau, aF_a(\tau))$. As $a \to 0$, the normalized

equation becomes $F' = 1 - F^2$, $F(0) = 0$, whose solution is $F(\tau) = \tanh \tau$. Figure 3 compares the two profiles.

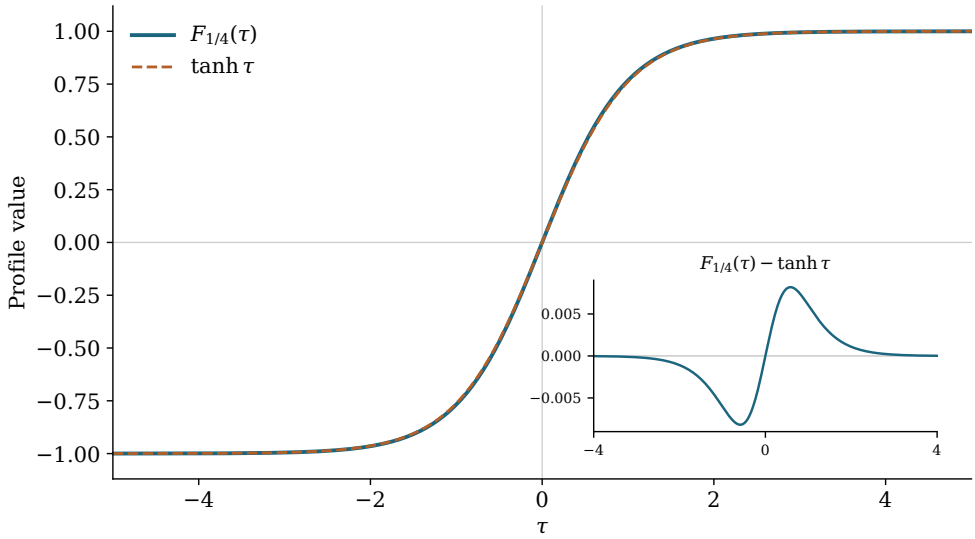


Figure 3: The standard transition profile $F_a$ for $a = 1/4$ and its limit $\tanh \tau$ as $a \to 0$. The inset shows their difference.

For the rescaled fields in (6.13), $b_n^4/A_n^2 = a^2$, so $C_n = 1 - \kappa_n V_n$. For every fixed spatial bound $D_0$, taking $a$ sufficiently small gives

$$c_a(u) \geq 7/8 \qquad (|u| \leq D_0). \tag{8.1}$$

For example, it is enough to impose

$$a^2(1 + D_0^2)^2 \leq \tfrac{1}{4}.$$

This is the field-domain part of the final choice of $a$: the spatial argument fixes $D_0$ first, and then this explicit inequality makes the uncorrected clock component at least $7/8$ on the whole attained band. The later inward correction leaves it at least $3/4$. The square root in $v_a$ is then real and smooth on that interval. The factor $1 - u^2$ makes its signed continuation smooth across $u = \pm 1$. Thus the fields are available on every fixed rescaled band once $a$ is sufficiently small.

**Lemma 8.2** (Scaling the single-cell model)**.** *Set*

$$\widetilde{f}_n(t) = b_n F_a((t - t_n)/h_n).$$

*This graph is strictly increasing, tends to $\pm b_n$ with vanishing slope at the two ends of the clock line, and satisfies*

$$\frac{1}{\sqrt{1 + (\widetilde{f}_n')^2}} + \frac{(\widetilde{f}_n^2 - b_n^2)^2}{2A_n^2} = 1, \qquad \frac{(1, \widetilde{f}_n')}{\sqrt{1 + (\widetilde{f}_n')^2}} = \mathbf{v}_n(\widetilde{f}_n). \tag{8.2}$$

*Moreover,*

$$\frac{d}{dt} P_n(\widetilde{f}_n(t)) = -C_n'(\widetilde{f}_n(t)) = \kappa_n V_n'(\widetilde{f}_n(t)). \tag{8.3}$$

*Proof.* Write $g_a$ for the reference graph of Section 3, retaining $V, C, P$ for its potential and fields. The definitions give $g_a(\tau) = aF_a(\tau)$ and

$$\begin{gathered} \widetilde{f}_n(t) = h_n g_a((t - t_n)/h_n), \qquad V_n(x) = h_n^4 V(x/h_n), \qquad \kappa_n = h_n^{-4}\kappa, \\ (C_n, P_n)(x) = (C, P)(x/h_n) \quad (|x| < b_n). \end{gathered} \tag{8.4}$$

The horizontality calculation in Proposition 3.1 gives the unit velocity $(C(g_a), P(g_a))$. Scaling clock and space by the same factor preserves slopes, so this identity and $C = 1 - \kappa V$ give (8.2). The same calculation gives $\frac{d}{d\tau}P(g_a) = -C'(g_a)$. With $\tau = (t - t_n)/h_n$, the chain rule yields

$$\frac{d}{dt}P_n(\widetilde{f}_n(t)) = \frac{1}{h_n}\frac{d}{d\tau}P(g_a(\tau)) = -\frac{1}{h_n}C'(g_a(\tau)) = -C_n'(\widetilde{f}_n(t)).$$

Together with $C_n = 1 - \kappa_n V_n$, this proves (8.3). Monotonicity and the endpoint limits are inherited from the transition of Section 3. □

The pulse and coefficient estimates must be uniform in the parameter $a$. The following two lemmas provide the profile bounds used below.

**Lemma 8.3** (Uniform bounds for the profile factor)**.** *For $0 < a \le 1/4$ and $|\widehat{x}| \le 1$, set*

$$u = \frac{a^2(1-\widehat{x}^2)^2}{4}, \qquad \omega_a(\widehat{x}) = \frac{\sqrt{1-u}}{1-2u}.$$

*Then $\omega_a \ge 1$, and for every integer $k \ge 0$, $\|\omega_a^{(k)}\|_{L^\infty([-1,1])} \le C_k$, with constants independent of $a$.*

*Proof.* Here $0 \le u \le 1/64$, so the denominator is positive and bounded away from zero. Since $1 - 2u \ge 0$, the inequality $\sqrt{1-u} \ge 1 - 2u$ follows by squaring and using $u(3 - 4u) \ge 0$. The uniform derivative bounds follow by differentiating this smooth expression on the compact range $0 \le u \le 1/64$; all derivatives of $u$ in $\widehat{x}$ are uniformly bounded. □

**Lemma 8.4** (Decay of the transition profile)**.** *For every integer $k \ge 1$ there is $C_k$, independent of $a$, such that*

$$1 - F_a(\tau)^2 + |F_a^{(k)}(\tau)| \le C_k e^{-2|\tau|} \qquad (\tau \in \mathbb{R}).$$

*Proof.* By Lemma 8.3 and (6.5), on $[-1, 1]$

$$\frac{v_a(\widehat{x})}{c_a(\widehat{x})} = (1 - \widehat{x}^2)\omega_a(\widehat{x}), \qquad \omega_a(\widehat{x}) \ge 1.$$

Thus (6.4) gives

$$\frac{d}{d\tau}\operatorname{arctanh} F_a(\tau) = \omega_a(F_a(\tau)).$$

Since $F_a$ is odd, $|F_a(\tau)| \ge \tanh|\tau|$. It follows that $1 - F_a(\tau)^2 \le 4e^{-2|\tau|}$. Each derivative $F_a^{(k)}$ is $1 - F_a^2$ times a uniformly bounded smooth function of $F_a$. For $k = 1$ this follows from the profile equation; differentiating that expression proves the assertion by induction, using Lemma 8.3. □

## 8.2 Localization and pulse energy

The fourth power in the definition of $\beta$ controls its derivatives where the pulse returns to zero.

**Lemma 8.5** (A cutoff for the pulse)**.** *The cutoff $\beta = \theta_\beta^4$ fixed in Section 6 satisfies*

$$|\beta'| + |\beta''| \le C\sqrt{\beta}. \tag{8.5}$$

*Proof.* Each term in the first two derivatives contains at least $\theta_\beta^2 = \sqrt{\beta}$ as a factor, and the remaining factors are bounded. □

On the plateau $|t-t_n| \le \ell_n/2$, we have $\beta_n = 1$, $\Phi_n = V_n$, and $f_n = \widetilde{f}_n$. Lemma 8.2 therefore gives

$$\mathbf{v}_n(f(t)) = \mathbf{h}_*(t) \quad (|t-t_n| \le \ell_n/2). \tag{8.6}$$

$$\mathbf{v}_n(x) = (C_n(x), P_n(x)), \qquad C_n(x) = 1 - \kappa_n V_n(x), \qquad C_n^2 + P_n^2 = 1. \tag{8.7}$$

The density formula also gives

$$Q_n(t,f) = \Phi_n(t,f), \qquad \partial_x Q_n(t,f) = \kappa_n^{-1} p_n' \tag{8.8}$$

On the plateau, (8.3) gives $p_n' = \kappa_n \partial_x \Phi_n(t,f)$, so the linear correction vanishes.

The explicit scales satisfy

$$t_{n+1} = t_n/2, \qquad \ell_n = t_n/16, \qquad |G_n| = 13t_n/32. \tag{8.9}$$

$$h_n/\ell_n \longrightarrow 0, \qquad h_{n+1} \le h_n/2. \tag{8.10}$$

Here and below, constants are uniform for $0 < a \le 1/4$, unless a dependence is indicated. In particular, $\sum_{n \ge l} h_n \le 2h_l$, after increasing $n_0$. The next estimates control both the reference length and its slopes.

**Lemma 8.6** (Pulse estimates for the chosen data)**.** *For the pulses* (6.9)*,*

$$\|f_n\|_\infty \le Cb_n, \qquad \|f_n'\|_\infty \le Ca, \qquad \int_{I_n} |f_n'|^2 \, dt \le Ca^2 h_n. \tag{8.11}$$

*Moreover, with* $\tau_n = t_n$ *and* $s_a = a\sqrt{1-a^2/4}/(1-a^2/2) > 0$*,*

$$f_n'(\tau_n) \longrightarrow s_a, \qquad -\varepsilon_n \le f_n'(t) \le s_a + \varepsilon_n, \qquad \varepsilon_n \longrightarrow 0. \tag{8.12}$$

*Proof.* Since $|F_a| \le 1$, we have $|f_n| \le b_n$. Differentiating (6.9) gives

$$|f_n'| \le \frac{b_n}{\ell_n}\|\beta'\|_\infty + \frac{b_n}{h_n}\|F_a'\|_\infty \le Ca.$$

Here $h_n \le \ell_n$, and Lemma 8.4 bounds $F_a'$ uniformly in $a$. Squaring the two product-rule terms and changing variables at their respective scales yields

$$\int_{I_n} |f_n'|^2 \, dt \le 2a^2 h_n \|F_a'\|_{L^2(\mathbb{R})}^2 + 2a^2 \frac{h_n^2}{\ell_n}\|\beta'\|_{L^2(\mathbb{R})}^2 \le Ca^2 h_n.$$

These are precisely (8.11).

At $t_n$, the profile equation gives $f_n'(t_n) = s_a$. On the plateau, write $w = 1 - u^2 \in [0,1]$. The numerator $w\sqrt{1 - a^2 w^2/4}$ is increasing in $w$, while its positive denominator $1 - a^2 w^2/2$ is decreasing. Hence $0 \le f_n' \le s_a$ there. Off the plateau, Lemma 8.4 and the product rule give

$$|f_n'| \le Ca\left(h_n/\ell_n + e^{-\ell_n/h_n}\right) \longrightarrow 0.$$

Taking this upper bound as $\varepsilon_n$ verifies (8.12). □

$$e_t = (1,0) \quad \text{on every gap}, \qquad u_a = (1 - a^2/2,\, a\sqrt{1-a^2/4}) \quad \text{at every center}. \tag{8.13}$$

### 8.3 Smooth extension of the coefficients

The narrow transition has large higher derivatives. In the coefficients of the frame, its core contributions cancel exactly; off the core, the exponential profile tails control the derivative losses.

**Lemma 8.7** (The reference coordinate at zero)**.** *The reference coordinate $r_*$ from (4.1) satisfies, on every cell,*

$$|r_*| \le Ca^3h_n^4.$$

*In particular $r_*'(0) = 0$. More generally $r_*$ extends across zero as a $C^3$ function with its first three derivatives zero there.*

*Proof.* Fix $t \in I_n$. Since $|F_{a,n}| \le 1$, the definitions (6.9) and (6.21) give

$$|f(t)| \le b_*(t) \le b_n, \qquad 0 \le A_*(t) \le A_n, \qquad 0 \le b_*(t)^2 - f(t)^2 \le b_n^2.$$

Thus (6.22) and (6.12) give

$$|q(t, f(t))| \le A_n^2 + \tfrac{1}{2}b_n^4 = a^2h_n^4(1 + \tfrac{1}{2}a^2).$$

Lemma 8.6 gives $|f'| \le Ca$. Multiplying this by the preceding estimate proves the bound on $r_* = q(t, f)f'$. The reference coordinate vanishes off the cells. On $I_n$,

$$\frac{|r_*(t)|}{t} \le \frac{16Ca^3h_n^4}{15t_n} \longrightarrow 0,$$

which proves $r_*'(0) = 0$.

For higher derivatives use the cell formula

$$q(t, f(t)) = A_n^2\beta_n^2 - \tfrac{1}{2}b_n^4\beta_n^4(1 - F_{a,n}^2)^2.$$

Each differentiation of a rescaled factor costs at most $C_k/h_n$ by Lemma 8.4 and $h_n \le \ell_n$. Differentiating this formula and the two terms of $f_n'$ therefore gives

$$\|r_*^{(k)}\|_{L^\infty(I_n)} \le C_k a^3 h_n^{4-k}.$$

For $k \le 3$ these derivatives tend to zero at the accumulation point. For $k \le 2$ the same bounds divided by $t_n$ still tend to zero. Successive difference quotients now give the claimed $C^3$ extension. □

**Lemma 8.8** (Checking both core cancellations)**.** *On $|t - t_n| \le \ell_n/2$, the chosen data satisfy*

$$\mathbf{h}_* = (c_a(F_{a,n}), av_a(F_{a,n})), \qquad r_* = A_n^2 p, \qquad q(t, f) = A_n^2 c. \tag{8.14}$$

*Both $e$ and the linear correction coefficient in (6.16) vanish there.*

*Proof.* On the plateau, $f = \widetilde{f}_n$, $q = A_n^2C_n$, and $\rho_- = 0$. Lemma 8.2 gives $\mathbf{h}_* = \mathbf{v}_n(f)$ and $f' = P_n(f)/C_n(f)$. Applying Proposition 4.1 with $\omega = A_n^2$ gives $r_* = A_n^2 p$ and $e = 0$, while $q(t, f) = A_n^2 c$. The linear correction vanishes by (8.3) and $\Phi_n = V_n$ on the plateau. □

To pass from these cellwise formulas to smooth coefficients at zero, we use the following extension lemma.

**Lemma 8.9** (Flat extension from disjoint supports)**.** *Suppose smooth functions $g_n(t, z)$ have pairwise disjoint clock supports contained in intervals where $t \asymp t_n$, with $t_n \downarrow 0$. For every compact set of state variables $z$, every multiindex $\alpha$, and every integer $N \ge 0$, suppose*

$$\|\partial^\alpha g_n\|_\infty = o(t_n^N). \tag{8.15}$$

*Then $\sum_n g_n$, extended by zero at $t \le 0$, is smooth and has zero Taylor jet along $t = 0$.*

*Proof.* Away from zero the sum is locally finite. The estimates with $N = 0$ give continuity at zero of the proposed derivatives. The estimates with $N = 1$, together with $t \asymp t_n$, show that their clock difference quotients tend to zero. Derivatives in the state variables are obtained in the same way, using the uniform estimates on compact sets. Induction on the total derivative order proves the claim. □

For the fixed function $q_0(x) = -x^4/2$, the cellwise coefficient families to which we apply the lemma are

$$(q - q_0)|_{I_n}, \qquad e|_{I_n}, \qquad m_n Q_n(t, x), \qquad m_n \chi_n(t)(W - w_n)^2. \tag{8.16}$$

The state variables are $x$ or $W$, as appropriate. The function $\rho_-$ is smooth and flat at zero by definition.

**Lemma 8.10** (Derivative bounds for the coefficients)**.** *The four coefficient families in* (8.16) *satisfy the estimates* (8.15)*, uniformly on compact sets of the state variables. The resulting coefficients and their first derivatives are bounded uniformly for* $0 < a \le 1/4$ *on a fixed compact neighborhood.*

*Proof of Lemma 8.10.* Fix a derivative order $\nu$. Constants may depend on $\nu, \beta$, and are uniform for $0 < a \le 1/4$. We check the estimates of Lemma 8.9 for each family in (8.16).

Direct differentiation gives

$$\|b_*^{(\nu)}\|_{L^\infty(I_n)} \le C_\nu a h_n \ell_n^{-\nu}, \qquad \|A_*^{(\nu)}\|_{L^\infty(I_n)} \le C_\nu a h_n^2 \ell_n^{-\nu}. \tag{8.17}$$

By (6.1), these satisfy (8.15). Thus $q(t, x) + x^4/2$ is smooth and flat in $t$, uniformly with its mixed derivatives on compact sets of $x$.

Fix $\theta > 0$ and restrict to $t \in I_n$ with $|t - t_n| \ge \theta \ell_n$. Lemma 8.4, rescaled by $h_n$, gives

$$\max_{0 \le k \le \nu} \left|\partial_t^k (F_{a,n}(t) - \operatorname{sgn}(t - t_n))\right| \le \mathcal{E}_{n,\nu}, \qquad \mathcal{E}_{n,\nu} = C_{\theta,\nu} h_n^{-N_\nu} e^{-c_{\theta,\nu}\ell_n/h_n}.$$

Here $N_\nu$ may be increased to absorb fixed derivative losses. These errors also satisfy (8.15).

On the plateau, (8.14) gives $e = 0$ exactly. Outside the plateau put $\varepsilon = \operatorname{sgn}(t - t_n)$. After adjusting the constants in $\mathcal{E}_{n,\nu}$, the four differences

$$f - \varepsilon b_n \beta_n, \quad q(t, f) - A_n^2 \beta_n^2, \quad r_* - \varepsilon A_n^2 b_n \beta_n^2 \beta_n', \quad q_x(t, f)$$

are bounded in $C^\nu$ by $\mathcal{E}_{n,\nu}$. Applying the corresponding estimates through order $\nu + 1$ to $e = r_*' + q_x(t, f)$ gives

$$\|e^{(\nu)}\|_{L^\infty(I_n)} \le C_\nu a^3 h_n^5 \ell_n^{-\nu-2} + \mathcal{E}_{n,\nu}. \tag{8.18}$$

Hence $e$ is smooth and flat. The term $\rho_-(t)x$ has the same property by definition.

The potential $\Phi_n$ is polynomial in $x$, with smooth cutoff coefficients. The linear coefficient $2A_n^2 p_n' - \partial_x \Phi_n(t, f)$ vanishes on the plateau. Outside it, $\partial_x \Phi_n(t, f)$ and $f' - \varepsilon b_n \beta_n'$ have $C^\nu$ norms bounded by $\mathcal{E}_{n,\nu}$, with the same convention on constants. On this outer region the $\nu$-th derivative of $p_n'$ is therefore bounded by $C_\nu a h_n \ell_n^{-\nu-2} + \mathcal{E}_{n,\nu}$. This controls both polynomial coefficients of the linear correction. The coefficient $K_n$ vanishes on $|t - t_n| \le \ell_n/8$. Thus its products with $f$ and $f^2$ involve the profile only where $F_{a,n}$ can be replaced by $\operatorname{sgn}(t - t_n)$ with the preceding exponentially small error. The derivatives of $K_n$ cost powers of $\ell_n^{-1}$, with constants depending on the fixed cutoffs. After multiplication by $m_n$, each fixed mixed derivative of an observation coefficient is bounded by $C_\nu m_n \ell_n^{-N_\nu} + \mathcal{E}_{n,\nu}$ on compact state sets, so the observation sum is smooth and flat.

Finally, the reference rate satisfies

$$0 \le Q_n(t, f) = b_n^4 \beta_n^5 (1 - F_{a,n}^2)^2 \le b_n^4.$$

Since $\sum_n m_n b_n^4 \ell_n < \infty$, the gap values $w_n$ are bounded. On compact sets of $W$, the clock derivatives of $m_n \chi(t/t_n)(W - w_n)^2$ are bounded by $C_\nu m_n t_n^{-\nu}$; the same holds for mixed derivatives. Their supports are disjoint, so Lemma 8.9 applies. The remaining terms are polynomial in the state variables. All displayed estimates are uniform in $a$, including derivative orders zero and one. On a fixed compact coordinate neighborhood they therefore also give the required uniform coefficient bounds. □

Consequently the frame is smooth, and its difference from the frame with $q = q_0$, $e = \rho_- = 0$, and zero observation sums is flat at the origin.

### 8.4 Bracket generation

Flat coefficient changes preserve every bracket value at the origin. In the coordinate $\zeta = \xi + x^5/10$, the limiting fields are

$$\begin{aligned} X_1^0 &= \partial_t + 2x^3\partial_r - r\partial_\zeta + (\zeta - x^5/10)^6\partial_W + (\zeta - x^5/10)^{10}\partial_Z, \\ X_2^0 &= \partial_x. \end{aligned} \tag{8.19}$$

**Lemma 8.11.** *The frame (6.24) is bracket-generating near the origin. Brackets of length at most 51 suffice at the origin.*

*Proof.* On $x = 0$, the polynomial fields satisfy

$$T = \operatorname{ad}_{X_2^0}^3 X_1^0 = 12\partial_r, \qquad V_0 = [T, X_1^0] = -12\partial_\zeta.$$

Indeed the third $x$-derivative of $2x^3$ is 12, while the third derivatives of $(\zeta - x^5/10)^6$ and $(\zeta - x^5/10)^{10}$ vanish at $x = 0$. Both $T$ and $X_1^0$ are tangent to this hypersurface, so their restrictions determine the restriction of their bracket. The same holds for repeated brackets with $V_0$. Therefore

$$\operatorname{ad}_{V_0}^6 X_1^0(0) = (-12)^6 6!\,\partial_W, \qquad \operatorname{ad}_{V_0}^{10} X_1^0(0) = (-12)^{10} 10!\,\partial_Z.$$

Together with $X_1^0(0), X_2^0(0), T(0), V_0(0)$, these give six independent directions, represented by bracket words of lengths $1, 1, 4, 5, 31, 51$. Flatness preserves their values for the actual frame. Their determinant is nonzero at the origin, hence on a smaller neighborhood. □

### 8.5 Differentiability of the curve and its velocity limits

The two conclusions here use different scales. The height $b_n = o(t_n)$ and the small tail length make the position have a first-order limit. The ratio $b_n/h_n = a$, together with (8.12), allows a nonvanishing slope on each narrow core. Thus differentiability is compatible with discontinuous velocity. Smoothness of the frame then transfers this planar behavior to the lifted curve; it does not smooth out the control oscillations.

**Lemma 8.12** (A tangent with discontinuous velocity)**.** *The curve (6.25) is differentiable at zero, with $\gamma'(0) = X_1(0)$. The cluster set of its right-hand unit controls is*

$$\left\{ \frac{(1, v)}{\sqrt{1 + v^2}} : 0 \le v \le s_a \right\}.$$

*Its arclength velocity has no continuous representative on an interval containing zero in its interior.*

*Proof.* If $t \in I_n$, the amplitude estimate gives $|f(t)|/t \le Cah_n/(t_n - \ell_n) \to 0$; on the gaps $f = 0$. The bounds on $f_n'$ make $f$ Lipschitz. The tail energy bound and the spacing of the cells give

$$0 \le s(t) - t \le \frac{1}{2}\int_0^t |f'(u)|^2\, du = o(t) \quad (t \downarrow 0).$$

For example, if $t$ lies in the cell $I_n$, or in its adjacent gap on the side of zero, the integral is at most $Ca^2h_n$ and $t \ge ct_n$.

The formula $r_* = q(t, f)f'$ tends to zero because $q(0, 0) = 0$ and $f'$ is bounded. On $t \ne 0$,

$$r_*' = e - q_x(t, f).$$

Smoothness of $e, q_x$ and $q_0'(0) = 0$ imply $r_*' \to 0$. Integrating this equality to zero gives $r_* = o(t)$. Flatness of the observation coefficients gives $W_*'(t) \to 0$ and $W_*(t) = o(t)$. The remaining two state coordinates vanish on the reference. Thus $\Gamma_a(t)/t \to (1, 0, 0, 0, 0, 0)$. Since $s(t)/t \to 1$, this proves the derivative assertion.

On every gap the spatial slope is zero. It tends to $s_a > 0$ at the selected points $\tau_n$. Continuity within each cell therefore produces every intermediate slope, and the bounds in (8.12) exclude other limits. The map $v \mapsto (1, v)/\sqrt{1 + v^2}$ gives the stated arc. Near each $\tau_n$, the spatial unit component is bounded away from zero on an open interval, while it is zero on the gaps. These intervals have positive arclength and accumulate at zero, so changing the velocity on a null set cannot make it continuous. The smooth frame transports these control limits to velocity limits in the horizontal plane at the origin. □

*Proof of Proposition 8.1.* Smoothness follows from Lemmas 8.9 and 8.10, bracket generation from Lemma 8.11, and the assertions about the velocity from Lemma 8.12. The reference satisfies the four horizontal laws on $t \ne 0$. The bounds just proved extend it across zero as an absolutely continuous horizontal curve.

For completeness, the abnormal lift is explicit. An abnormal extremal over a horizontal trajectory $\gamma$ with control $(u_1, u_2)$ is a nonzero cotangent curve $\alpha(s)$ annihilating the horizontal distribution and satisfying

$$\frac{d}{ds}\langle \alpha(s), Y(\gamma(s))\rangle = \sum_{i=1}^{2} u_i(s)\langle \alpha(s), [X_i, Y](\gamma(s))\rangle \quad \text{a.e.}$$

for every smooth local vector field $Y$ [1, 2, 21]. In coordinates $q^j$, this is the adjoint equation

$$\dot\alpha_j = -\sum_{i=1}^{2}\sum_{\ell} u_i\alpha_\ell\, \partial_{q^j} X_i^\ell(\gamma).$$

For (6.24), $X_2 Z = 0$ identically, and both $X_1 Z$ and its differential vanish on the reference. Indeed $\xi = 0$, $k \ge 2$, and $W = w_n$ on each gap test. Thus $\alpha(s) = dZ_{\gamma(s)}$ is an abnormal extremal with constant coordinate components. A normal extremal would have a smooth arclength-parametrized projection. The velocity discontinuity therefore makes the trajectory strictly abnormal. □

In the notation (8.13), the velocity conclusion is equivalently the following.

**Corollary 8.13** (Limiting velocity directions)**.** *The right-hand cluster set of* $\mathbf{h}_*(t)$ *is the closed arc in the first quadrant of the unit circle with endpoints* $e_t, u_a$ *from* (8.13)*. The arclength velocity of the horizontal lift has no continuous representative on an interval containing zero in its interior, although the curve is differentiable there with derivative* $X_1(0)$*.*

*Proof.* By Lemma 8.12, the slopes fill $[0, s_a]$. Its endpoint $(1, s_a)/\sqrt{1 + s_a^2}$ is precisely $u_a$ in (8.13). □

# 9 Comparison deficits and clock reversals

We compare the competitor with the cell subsolutions on finitely many cells and with the forward direction $e_t$ everywhere else. The excess length of the untreated reference pulses will be the tail in this comparison.

Fix a sufficiently large $j$ and a competitor of length $L \le L_*$, parametrized by planar arclength $s \in [0, L]$. Write

$$\mathbf{h} = (u_t, u_x) = (t', x'), \qquad |\mathbf{h}| = 1 \quad \text{a.e.}, \qquad B = \int (-u_t)_+ \, ds.$$

We also use the fixed clock defect

$$\mathfrak{B} = \int (1 - 2u_t)_+ \, ds, \qquad 2B \le \mathfrak{B} \le 2 \int (1 - u_t) \, ds, \qquad \mathfrak{B} \le 3L. \tag{9.1}$$

It counts slow forward motion as well as reversals. For small $a$, it vanishes on the reference, whose clock speed is $c \ge 3/4$.

The competitor's clock endpoints are $t_{\text{in}} = -t_j$ and $T_j$. Since $L_* = O(t_j)$, these competitors stay in a fixed compact coordinate neighborhood for large $j$: until a first exit the smooth ODE coefficients bound their full velocities, whereas their lengths tend to zero. All state coordinates and their arclength derivatives are therefore bounded uniformly in the competitor and $a$.

We write $\int g \, dt = \int g u_t \, ds$ for signed clock integrals, and $\Delta \int g \, dt$ for competitor minus reference integrals. A subscript $I_n$ on a path integral includes every visit to that cell. For a bounded function of clock alone, the signed integral is its primitive difference between endpoint clocks, even when the clock reverses.

## 9.1 The reference tail and the initial deficit

The reference excess on each cell and its tail are

$$\epsilon_n = \int_{I_n} (\sqrt{1 + f'^2} - 1) \, dt, \qquad \mathcal{T}_N = \sum_{n > N} \epsilon_n \quad (N \ge j - 1). \tag{9.2}$$

The pulse estimates (8.11) and $\sqrt{1 + z^2} - 1 \le z^2/2$ give

$$\|f'\|_{L^\infty(I_n)} \le Ca, \qquad \int_{I_n} |f'|^2 \, dt \le Ca^2 h_n, \qquad \sum_{n \ge l} h_n \le 2h_l. \tag{9.3}$$

The last bound follows by summing the geometric decrease in (8.10). Thus, for a fixed constant $C_T$ independent of $a, j, N$,

$$0 \le \mathcal{T}_N \le C_T a^2 h_{N+1}, \qquad L_* = (T_j - t_{\text{in}}) + \mathcal{T}_{j-1}. \tag{9.4}$$

**Lemma 9.1.** *For sufficiently large $j$, the competitor visits no cell of index below $j$. Its comparison with $e_t$ satisfies*

$$0 \le \Lambda_{j-1} := \int (1 - u_t) \, ds = L - (T_j - t_{\text{in}}) \le C_T a^2 h_j. \tag{9.5}$$

*Proof.* The equality follows by integration of $u_t$; the upper bound follows from $L \le L_*$ and (9.4). Pointwise, $2(-u_t)_+ \le 1 - u_t$, so $2B \le C_T a^2 h_j$. A visit to $I_{j-1}$, or any cell above it, would require backward clock variation at least $t_j/8$ to return to $T_j$. Since $h_j/t_j \to 0$, this is impossible for large $j$. □

### 9.2 Finite comparisons and the clock estimate

On each treated cell let $\mathbf{k}_n(t,x)$ be a measurable vector with

$$|\mathbf{k}_n| \le 1, \qquad (\mathbf{k}_n)_t \ge 3/4. \tag{9.6}$$

Section 12 constructs these vectors on the spatial regions obtained in Section 11. A comparison is defined when these conditions hold at every visited point of its treated cells. Set $\mathbf{k}^{(N)} = \mathbf{k}_n$ on $I_n$, $j \le n \le N$, and $\mathbf{k}^{(N)} = e_t$ elsewhere. Define

$$\Lambda_N = \int (1 - \mathbf{h}\cdot\mathbf{k}^{(N)})\, ds. \tag{9.7}$$

This agrees with (9.5) for the empty comparison. For every defined comparison,

$$\tfrac{1}{2}|\mathbf{h} - \mathbf{k}^{(N)}|^2 \le 1 - \mathbf{h}\cdot\mathbf{k}^{(N)}, \qquad 0 \le \Lambda_N \le 2L. \tag{9.8}$$

**Lemma 9.2.** *For every defined comparison and bounded nonnegative integrand $g$,*

$$\int g\, ds \le 2\int g\, dt + 4\|g\|_\infty \Lambda_N. \tag{9.9}$$

*For a subarc of length $L'$ and net clock displacement $\Delta t$,*

$$\mathfrak{B} \le 4\Lambda_N, \qquad L' \le 2|\Delta t| + 4\Lambda_N. \tag{9.10}$$

*On every untreated cell $I_n$, $n > N$,*

$$\int_{I_n} u_x^2\, ds \le 2\Lambda_N. \tag{9.11}$$

*Proof.* For $k_t \ge 3/4$, completing the square gives

$$2u_t + 2(u_t - k_t)^2 = 2(u_t - k_t + 1/2)^2 + 2k_t - 1/2 \ge 1.$$

Multiply by $g$, integrate, and use (9.8) to prove (9.9). The same pointwise inequality gives $(1-2u_t)_+ \le 2(u_t-k_t)^2 \le 4(1-\mathbf{h}\cdot\mathbf{k})$, which proves the bound for $\mathfrak{B}$. Taking $g$ to be the indicator of the subarc gives the bound for $L'$. Finally, on an untreated cell the deficit is $1-u_t$, and $u_x^2 = 1 - u_t^2 \le 2(1-u_t)$. □

## 10 Recovering cell integrals from the endpoints

The endpoint of $Z$ controls the observation errors directly in terms of the clock defect $\mathfrak{B}$. These estimates require no cell comparison field.

### 10.1 The nonnegative rate and its derivative

Set

$$\mathcal{E} = \xi^k + \sum_n m_n \chi_n(t)|W - w_n|^2, \qquad k = 10, \quad d = 6, \qquad \int \mathcal{E}\, dt = 0. \tag{10.1}$$

The last equality follows from the common $Z$-endpoints. The mechanism is a comparison of two sizes: the derivative bound below forces a peak of height $A$ to contribute at least order $A^{1+1/k}$ to its arclength integral, while the zero signed integral bounds that integral by $A\mathfrak{B}$. This forces

$A = O(\mathfrak{B}^k)$, independently of any cell subsolution. Initially $\xi = 0$ and the clock is negative, so $\mathcal{E} = 0$. The tests $\chi = \theta^{10}$ satisfy

$$|\chi_n'| \le c_n^\chi \chi_n^{1-1/k}, \qquad c_n^\chi = C t_n^{-1}, \qquad \sup_n m_n < \infty, \quad \sup_n m_n^{1/k} c_n^\chi < \infty. \tag{10.2}$$

The powers also satisfy

$$\tfrac{1}{2} + d/k = 11/10 \ge 1 - 1/k = 9/10. \tag{10.3}$$

**Lemma 10.1** (Endpoint bound for the rate of $Z$)**.** *Every competitor under consideration satisfies*

$$\max \mathcal{E} \le C\mathfrak{B}^k, \qquad \int \mathcal{E}\, ds \le C\mathfrak{B}^{k+1}, \qquad \|\xi\|_\infty \le C\mathfrak{B}. \tag{10.4}$$

*Proof.* On a gap every $Q_n$ vanishes, so $W' = \xi^d u_t$. For the active term $E_n = m_n \chi_n |W - w_n|^2$, differentiation of $\chi_n$ contributes at most

$$m_n^{1/k} c_n^\chi |W - w_n|^{2/k} E_n^{1-1/k} \le C\mathcal{E}^{1-1/k}.$$

The states are bounded on the fixed compact neighborhood, and the gap supports are disjoint. Differentiation of $W$ contributes at most

$$C\mathcal{E}^{1/2}|\xi|^d \le C\mathcal{E}^{1/2+d/k} \le C\mathcal{E}^{1-1/k},$$

by (10.3) and boundedness of $\mathcal{E}$. Since $\xi'$ is bounded, the derivative of $\xi^k$ has the same bound. Thus $|\mathcal{E}'| \le C\mathcal{E}^{1-1/k}$ almost everywhere.

Put $A = \max \mathcal{E}$. The zero signed integral gives

$$\int \mathcal{E}\, ds = 2\int \mathcal{E}\, dt + \int \mathcal{E}(1 - 2u_t)\, ds \le A\mathfrak{B}.$$

Integrating the derivative of $\mathcal{E}^{1+1/k}$ from its initial zero to a maximum yields

$$A^{1+1/k} \le (1 + 1/k) \int \mathcal{E}^{1/k} |\mathcal{E}'|\, ds \le C \int \mathcal{E}\, ds \le CA\mathfrak{B}.$$

For $A > 0$, division gives $A \le C\mathfrak{B}^k$; for $A = 0$ this is immediate. The integral bound follows by substitution, and $|\xi|^k \le \mathcal{E}$ gives the last assertion. □

## 10.2 A one-sided cell observation

Write $P_W = W - W_*(t)$ and $\omega = \sum_i m_i \chi_i$. Since $W_* = w_i$ on the support of $\chi_i$, $\mathcal{E} = \xi^{10} + \omega P_W^2$. For $n \ge j > n_0$, define

$$\zeta_n(t) = \int_{-\infty}^t \left( \frac{\chi_n(u)}{M_n} - \frac{\chi_{n-1}(u)}{M_{n-1}} \right) du. \tag{10.5}$$

The lower test precedes the upper one, so $0 \le \zeta_n \le 1$. It equals one on $I_n$, zero on every other cell, and zero at both endpoint clocks. Set

$$\rho = 11/2, \qquad R_n^{\mathrm{obs}} = m_n^{-1} \left( 1 + \frac{1}{M_n \sqrt{m_n}} + \frac{1}{M_{n-1}\sqrt{m_{n-1}}} \right), \qquad S_N = \sum_{n=n_0+1}^{N} \kappa_n R_n^{\mathrm{obs}}. \tag{10.6}$$

Dividing by $m_n$ recovers an unweighted cell integral; each adjacent test costs its inverse mass and the inverse square root of its weight. These are precisely the factors in $R_n^{\mathrm{obs}}$. Their growth is the price of the small weights used for smoothness. The sum $S_N$ includes the multipliers in the length identity. The scale choice will make both losses affordable.

**Proposition 10.2.** *For every $n \geq j$, independently of any cell comparison,*

$$\Delta_n := \Delta \int Q_n \, dt \leq C R_n^{\mathrm{obs}} \mathfrak{B}^{\rho}. \tag{10.7}$$

*Proof.* The auxiliary equation and the locally Lipschitz reference integral give

$$dP_W = \left[ \sum_i m_i (Q_i(t,x) - Q_i(t,f)) + \xi^6 \right] dt.$$

Integrating by parts, using $\zeta_n = 0$ at the endpoints, gives

$$m_n \Delta_n = -\int \zeta_n' P_W \, dt - \int \zeta_n \xi^6 \, dt. \tag{10.8}$$

On the test in $G_i$, for $i = n, n-1$,

$$|\zeta_n' P_W| \leq \frac{\sqrt{\chi_i}}{M_i \sqrt{m_i}} \sqrt{\mathcal{E}}.$$

Cauchy–Schwarz and (10.4), with $L \leq 1$, therefore yield

$$\begin{aligned} \left| \int \zeta_n' P_W \, dt \right| &\leq \left( \frac{1}{M_n \sqrt{m_n}} + \frac{1}{M_{n-1} \sqrt{m_{n-1}}} \right) \sqrt{L} \left( \int \mathcal{E} \, ds \right)^{1/2} \\ &\leq C \left( \frac{1}{M_n \sqrt{m_n}} + \frac{1}{M_{n-1} \sqrt{m_{n-1}}} \right) \mathfrak{B}^{11/2}. \end{aligned}$$

The other term has an unfavorable sign only during backward visits:

$$-\int \zeta_n \xi^6 \, dt \leq \|\xi\|_\infty^6 B \leq C \mathfrak{B}^7,$$

where $2B \leq \mathfrak{B}$. For large $j$, $\mathfrak{B} \leq 3L \leq 1$, so $\mathfrak{B}^7 \leq \mathfrak{B}^{11/2}$. Divide (10.8) by $m_n$ to conclude. □

### 10.3 Size of the observation errors

The same scale separation will control each cell error and their sum. Write

$$\nu_n = b_n^4, \qquad \mathcal{G}_n(t,x) = \frac{\Phi_n(t,x)}{b_n^4} = \beta_n(t)(x^2/b_n^2 - \beta_n(t)^2)^2. \tag{10.9}$$

Since $M_n = c_\chi t_n$, the logarithm of $R_n^{\mathrm{obs}}$ is $O(4^n + n)$, whereas $|\log h_n| = e^{n^2}$. Increasing $n_0$ gives

$$R_n^{\mathrm{obs}} \leq C h_n^{-1/4}, \qquad S_N \leq C a^{-2} \sum_{n=n_0+1}^{N} h_n^{-17/4} \leq C a^{-2} h_N^{-17/4}. \tag{10.10}$$

The sum is bounded by a fixed multiple of its largest term because successive terms grow at least geometrically. Consequently

$$S_N (a^2 h_N)^{9/2} \leq C a^7 h_N^{1/4} \longrightarrow 0. \tag{10.11}$$

The residual factor $h_N^{1/4}$ is the margin anticipated in Subsection 6.3: the quartic integral costs five powers of $h_n$, the observation gives $11/2$, and the weight loss uses $1/4$. The same estimate also controls the individual normalized errors, since

$$\kappa_n R_n^{\mathrm{obs}} \leq S_n, \qquad \kappa_n \nu_n h_n = a^2 h_n / 2. \tag{10.12}$$

# 11 From an integral to a spatial bound

The endpoint estimate controls a signed integral of $Q_n$. We first relate this density to the nonnegative quartic $\mathcal{G}_n$ from (10.9), and then use the spatial energy of a short competitor to control its largest value. This establishes the spatial band before the comparison field is used.

## 11.1 Bounds for the quartic density

The linear correction can make $Q_n$ negative. Its negative part is controlled by the same quadratic term already included in the construction.

**Lemma 11.1** (Cutoff estimates and the linear correction)**.** *The pulse cutoff satisfies*

$$|\beta'| + |\beta''| \le C\sqrt{\beta}. \tag{11.1}$$

*Let $R = \ell_n/h_n$ and let $L_n$ denote the coefficient of $y = x - f(t)$ in the linear correction to $\Phi_n$:*

$$L_n(t) = 2A_n^2 p_n'(t) - \partial_x \Phi_n(t, f(t)).$$

*Uniformly in $n$ and $a$, for every $t \in I_n$ and every $y \in \mathbb{R}$,*

$$|L_n(t)y| \le b_n^2 \vartheta_n(t) y^2 + C b_n^4 R^{-4}. \tag{11.2}$$

*Proof.* The derivative bound is (8.5). On the plateau $L_n = 0$ by Lemma 8.8. Off the plateau $\vartheta_n = \beta_n$. Abbreviate $h = h_n$, $\ell = \ell_n$, and $b = b_n$. Differentiate $f_n = b\beta_n F_{a,n}$ twice, using (11.1) on the rescaled cutoff and Lemma 8.4 on the profile. This gives

$$|p_n'| \le |f_n''| \le Ca\sqrt{\beta_n}\left(\frac{h}{\ell^2} + \frac{e^{-cR}}{\ell} + \frac{e^{-cR}}{h}\right) \le Ca\frac{h}{\ell^2}\sqrt{\beta_n}.$$

Moreover,

$$\partial_x \Phi_n(t, f) = -4b^3\beta_n^4 F_{a,n}(1 - F_{a,n}^2).$$

Using $e^{-cR} \le CR^{-2}$ and $A_n = ah^2$ yields

$$|L_n| \le Cb^3 R^{-2}\sqrt{\vartheta_n}.$$

Young's inequality proves (11.2). □

The density bounds are uniform over the cells and small $a$.

**Lemma 11.2.** *After increasing $n_0$, there is a constant $C$ such that, with $\delta_n = C(h_n/\ell_n)^4$, the following estimates hold:*

$$\nu_n \mathcal{G}_n(t,x) \le Q_n(t,x) + \delta_n \nu_n \le C\nu_n(1 + \mathcal{G}_n(t,x)) \qquad (t \in I_n), \tag{11.3a}$$

$$\delta_n \ell_n \le C h_n, \tag{11.3b}$$

$$0 \le \int_{I_n} Q_n(t, f(t))\, dt \le C\nu_n h_n. \tag{11.3c}$$

*For each $A < \infty$,*

$$\beta_n(t) = 1, \quad \mathcal{G}_n(t,x) \le A \quad \Longrightarrow \quad |x| \le \sqrt{1 + \sqrt{A}}\, b_n. \tag{11.4}$$

*There is a fixed $\delta_0 > 0$ such that the support of $\theta_\beta((t - t_n)/\ell_n)$, and hence of $\mathcal{G}_n$, lies in $|t - t_n| \le (1 - \delta_0)\ell_n$.*

*Proof.* Put $R = \ell_n/h_n$, $Y = (x-f)/b_n$, and use the function $\mathcal{G}_n$ in (10.9). Lemma 11.1 gives

$$Q_n + Cb_n^4 R^{-4} \geq b_n^4(\mathcal{G}_n + 3\vartheta_n Y^2) \geq b_n^4 \mathcal{G}_n. \tag{11.5}$$

On $\operatorname{supp}\eta_n'$, $\beta_n = 1$ and $\ell_n|\eta_n'| \leq C$; elsewhere $\vartheta_n = \beta_n(1-\eta_n) \leq \beta_n$. Thus $\vartheta_n \leq C\beta_n$. Since $|f|/b_n \leq \beta_n$,

$$\beta_n(x/b_n)^2 \leq \sqrt{\mathcal{G}_n} + 1, \qquad \vartheta_n Y^2 \leq C(1+\sqrt{\mathcal{G}_n}).$$

The same linear-correction estimate gives the upper bound

$$Q_n + Cb_n^4 R^{-4} \leq Cb_n^4(1+\mathcal{G}_n).$$

Take $\delta_n = CR^{-4}$. Then $\delta_n \ell_n/h_n = CR^{-3} \to 0$. Moreover,

$$\begin{aligned} 0 \leq \int_{I_n} Q_n(t, f(t))\,dt &= b_n^4 \int_{I_n} \beta_n^5 (1 - F_{a,n}^2)^2\,dt \\ &\leq b_n^4 h_n \int_{\mathbb{R}} (1 - F_a(\tau)^2)^2\,d\tau \leq Cb_n^4 h_n. \end{aligned}$$

This proves (11.3).

Where $\beta_n = 1$, $\mathcal{G}_n = (x^2/b_n^2 - 1)^2$. Its sublevel set $\mathcal{G}_n \leq A$ satisfies

$$|x|/b_n \leq \sqrt{1+\sqrt{A}}.$$

This proves (11.4). The support of $\beta$ is a compact subset of $(-1,1)$, giving the required fixed support margin for $\mathcal{G}_n$.

□

The same calculation explains the rejection of the whole-pulse chord in Figure 2(a). On the plateau, the chord has potential integral $b_n^4 \ell_n$, whereas the reference has

$$\int_{|t-t_n| \leq \ell_n/2} \Phi_n(t, f(t))\,dt \leq b_n^4 h_n \int_{\mathbb{R}} (1 - F_a(\tau)^2)^2\,d\tau \leq Cb_n^4 h_n.$$

The normalized density on the chord is $\mathcal{G}_n(t,0) = \beta_n^5$. Thus the lower bound in (11.3), with $R = \ell_n/h_n$, also gives

$$\int_{I_n} Q_n(t,0)\,dt \geq b_n^4 \ell_n (1 - 2CR^{-4}) > \int_{I_n} Q_n(t, f(t))\,dt$$

for large $n$. Proposition 5.1 therefore excludes this chord in any competitor with strictly increasing clock and the prescribed observation endpoints. The short planar length of a chord is incompatible with the integral recovered by the general observation mechanism.

### 11.2 A peak estimate in arclength

The fourth-power cutoff permits a direct estimate of the weighted spatial coordinate along the competitor. This will control every visit to a cell without selecting visits according to their clock order.

**Lemma 11.3.** *Fix $M \geq 1$. Suppose the comparison before $I_n$ is defined and $\Lambda_{n-1} \leq Ma^2 h_n$. For each fixed $a > 0$ and sufficiently large $j$, uniformly for $n \geq j$,*

$$U_n := \max_s \mathcal{G}_n(t(s), x(s)) \leq C_M + \frac{C_M}{h_n} \int \mathcal{G}_n(t(s), x(s))\,ds. \tag{11.6}$$

*Proof.* Write $\theta = \theta_\beta$, so $\beta = \theta^4$. Nonnegativity of $\theta$ and boundedness of $\theta''$ imply

$$|\theta'|^2 \le 2\|\theta''\|_\infty \theta. \tag{11.7}$$

Indeed, for $D = \|\theta''\|_\infty > 0$, Taylor's upper bound at $u - \theta'(u)/D$ gives $0 \le \theta(u - \theta'(u)/D) \le \theta(u) - \theta'(u)^2/(2D)$.

Suppress the cell index and set

$$\sigma = s/h, \qquad z(\sigma) = \theta((t(h\sigma) - t_n)/\ell)\frac{x(h\sigma)}{b}, \qquad H = \max|z|.$$

The competitor stays in the fixed coordinate neighborhood; choose $R$ with $|x| \le R$ there. Differentiating and using (11.7), $|u_t| \le 1$, and $b = ah$ yields

$$|z_\sigma| \le \frac{|u_x|}{a} + C\frac{h}{\ell}\sqrt{\frac{|x|}{b}}\sqrt{|z|} \le \frac{|u_x|}{a} + \varepsilon_n\sqrt{|z|}, \qquad \varepsilon_n = C\frac{\sqrt{Rh_n/a}}{\ell_n}. \tag{11.8}$$

For fixed $a > 0$, the scales (6.1) give $\varepsilon_n \to 0$. Choose $j$ so that $\varepsilon_n \le 1$ for all $n \ge j$. On the untreated cell, (9.11) gives

$$\int_{t\in I_n}\left|\frac{u_x}{a}\right|^2 d\sigma = \frac{1}{a^2h_n}\int_{I_n} u_x^2\,ds \le 2M.$$

If $H > 0$, let $s_* = h\sigma_*$ attain it. Then $t(s_*)$ lies in the support of $t \mapsto \theta((t-t_n)/\ell_n)$, at distance at least $\delta_0\ell_n$ from both cell boundaries. Since the terminal clock lies above $I_n$, $L - s_* \ge T_j - t(s_*) \ge \delta_0\ell_n$. For large $j$, $h_n < \delta_0\ell_n$. Thus the whole arclength interval $[s_*, s_* + h_n]$ exists and remains in $I_n$, because $|t(s) - t(s_*)| \le |s - s_*|$. Integrating (11.8) and applying Cauchy–Schwarz on this interval gives

$$|z(\sigma) - z(\sigma_*)| \le \sqrt{2M} + \sqrt{H} \qquad (\sigma_* \le \sigma \le \sigma_* + 1).$$

Either $H \le C_M$, or the right side is at most $H/2$. In the latter case $|z| \ge H/2$ throughout this interval. For every point, putting $X = x/b$,

$$|z|^4 = \beta X^4 \le 2\mathcal{G}_n + 2, \qquad \mathcal{G}_n = \beta(X^2 - \beta^2)^2 \le 2|z|^4 + 2.$$

Integration over the interval of arclength $h_n$ therefore gives $H^4/16 \le 2h_n^{-1}\int \mathcal{G}_n\,ds + 2$. This proves (11.6) in both cases; $H = 0$ is immediate. The bound $C_M$ is independent of $R, a, n$; these enter only the choice of the starting index. □

**Lemma 11.4** (Spatial bounds on a new cell)**.** *Fix $M \ge 1$. For sufficiently small fixed $a > 0$ and sufficiently large $j$, suppose the comparison through $n-1$ is defined and*

$$\Lambda_{n-1} \le Ma^2h_n, \qquad \Delta_n \le \nu_n h_n, \qquad n \ge j.$$

*Then*

$$\mathcal{G}_n(t(s), x(s)) \le C_M, \qquad \int \mathcal{G}_n(t(s), x(s))\,ds \le C_M h_n. \tag{11.9}$$

*In particular $|x| \le D_0(M)b_n$ on $\{\beta_n = 1\}$ at every visit.*

*Proof.* The current comparison equals $e_t$ on $I_n$. With $\Lambda = \Lambda_{n-1}$, equation (9.11) gives

$$\frac{1}{a^2h_n}\int_{I_n} u_x^2\,ds \le \frac{2\Lambda}{a^2h_n} \le 2M. \tag{11.10}$$

Add the constant padding in (11.3) on the cell and set the result to zero outside it. The assumption on $\Delta_n$ and (11.3c) bound its signed integral above by $C\nu_n h_n$, since the endpoints straddle $I_n$ and $\delta_n|I_n| \le Ch_n$. Equation (11.3a) bounds its maximum by $C\nu_n(1+U_n)$. Applying (9.9) to this nonnegative function therefore gives

$$\frac{1}{h_n}\int \mathcal{G}_n\,ds \le C + C\frac{\Lambda}{h_n}(1+U_n) \le C + C_M a^2(1+U_n). \tag{11.11}$$

Lemma 11.3 applies by (11.10). Combining its bound with the preceding inequality yields

$$U_n \le C_M + C_M a^2(1+U_n).$$

Choose $a$ so that $C_M a^2 \le 1/2$ and absorb. The resulting peak bound is at most $2C_M + 1$. The integral bound follows by substitution, and (11.4) gives the spatial band. □

# 12 Hamilton–Jacobi subsolutions and finite length comparisons

The autonomous Hamilton–Jacobi subsolution of Section 3, rescaled by (8.4), already gives the exact comparison on the core. We extend it through the return portions and verify that the comparison vector stays in the unit ball on the entire attained spatial sublevel. We then sum the cell length identities.

## 12.1 A smooth Hamilton–Jacobi subsolution on a cell

Fix $B_0 > 1$. A smooth function $\Psi_n$ on $\mathcal{G}_n < B_0$ is a subsolution if

$$\mathbf{k}_n = (1 + \partial_t\Psi_n - \kappa_n Q_n, \partial_x\Psi_n), \qquad |\mathbf{k}_n| \le 1, \qquad (\mathbf{k}_n)_t \ge 3/4. \tag{12.1}$$

In the induction this open sublevel will strictly contain every attained point of the cell.

**Lemma 12.1.** *For every $B_0 > 1$, sufficiently small $a > 0$, and sufficiently large $n$, there is a smooth subsolution $\Psi_n$ on $\mathcal{G}_n < B_0$, constant independently of $x$ on each side of $I_n$, such that*

$$\mathbf{k}_n(t, f(t)) = \mathbf{h}_*(t). \tag{12.2}$$

*Proof.* Suppress the index and put $y = x - f(t)$. On $\operatorname{supp}\eta$ we have $\beta = 1$, so the sublevel bound gives $|x| \le D_0 b$, with $D_0 = \sqrt{1+\sqrt{B_0}}$. Let $\Psi'_{\mathrm{mod}} = P_{\mathrm{mod}}$ be the primitive from the proof of Proposition 3.1, with subscripts denoting the model. On $|x| < b$, set $\Psi^0(x) = h\Psi_{\mathrm{mod}}(x/h)$; then $(\Psi^0)' = P$ by (8.4). Integrating the signed smooth continuation of $P$, justified by (8.1), extends this primitive to an interval slightly larger than $[-D_0 b, D_0 b]$. Since $P' = h^{-1}v_a'(x/b)$, for small $a$,

$$|P'| \le C_{B_0}/h, \qquad R_\Psi(t,x) := \Psi^0(x) - \Psi^0(f) - py, \qquad |R_\Psi| \le C_{B_0}y^2/h. \tag{12.3}$$

Here $P(f) = p$ on the plateau. The product $\eta R_\Psi$ is extended by zero outside that plateau. Choose $\psi_0$ by $\psi_0' = \sqrt{1+f'^2} - 1 + \kappa Q(t,f)$, and set

$$\Psi = \psi_0(t) + p(t)y + \eta(t)R_\Psi(t,x). \tag{12.4}$$

The localized product is smooth. Outside the cell, $f, p, Q$ vanish, $\psi_0' = 0$, and hence $\Psi$ is a spatial constant on either side.

Let $\overline{\mathbf{k}} = (1-\eta)\mathbf{h}_* + \eta\mathbf{v}(x)$, with the second term evaluated only on its support. Define

$$\mathcal{R} = (1-\eta)[\Phi(t,x) - \Phi(t,f) - \Phi_x(t,f)y] + 4b^2\vartheta y^2, \qquad D = \kappa\mathcal{R} - \eta' R_\Psi.$$

Differentiation of (12.4) gives $\Psi_x = (1-\eta)p + \eta P$. On the plateau, $\partial_t R_\Psi = -p'y$, and (8.3) gives $p' = \kappa\Phi_x(t,f)$. Everywhere, $1 + \psi_0' - pf' - \kappa Q(t,f) = c$. Substitution of (6.16) therefore gives

$$(1 + \Psi_t - \kappa Q, \Psi_x) = \overline{\mathbf{k}} - De_t. \tag{12.5}$$

Outside $\operatorname{supp}\eta$ the same identity follows directly with $\eta = \eta' = 0$.

To bound $D$, expand the quartic exactly:

$$\begin{aligned}\mathcal{R} &= (1-\eta)\beta(x^2-f^2)^2 \\ &\quad + [4b^2\vartheta - 2(1-\eta)\beta(b^2\beta^2 - f^2)]y^2 \geq 2b^2\vartheta y^2.\end{aligned} \tag{12.6}$$

Indeed $0 \leq b^2\beta^2 - f^2 \leq b^2$ and $\vartheta \geq \beta(1-\eta)$. On the whole sublevel, including where $\beta$ is small,

$$\beta(x^2-f^2)^2 \leq 2b^4\mathcal{G} + 2b^4, \qquad \vartheta y^2 \leq C_{B_0} b^2.$$

The second bound follows from $\vartheta \leq C\beta$, $|f|/b \leq \beta$, and $\beta(x/b)^2 \leq \sqrt{\mathcal{G}} + 1$. Thus $0 \leq \kappa\mathcal{R} \leq C_{B_0}a^2$. By $\ell|\eta'| \leq \vartheta$, (12.3), and $2\kappa b^2 = h^{-2}$,

$$|\eta' R_\Psi| \leq \frac{C_{B_0}\vartheta y^2}{h\ell} \leq C_{B_0}\frac{h}{\ell}\kappa\mathcal{R}.$$

For large $n$, this proves

$$\tfrac{1}{2}\kappa\mathcal{R} \leq D \leq \tfrac{3}{2}\kappa\mathcal{R} \leq C_{B_0}a^2. \tag{12.7}$$

For small $a$, both unit vectors forming $\overline{\mathbf{k}}$ have clock component at least $7/8$ on their domains. Hence $|\overline{\mathbf{k}}| \leq 1$, and we may also arrange $D \leq 1/8$. Equation (12.5) then gives $k_t \geq 3/4$ and

$$|\mathbf{k}|^2 = |\overline{\mathbf{k}}|^2 - D(2\overline{k}_t - D) \leq 1.$$

On the reference $R_\Psi = \mathcal{R} = 0$, and both active unit vectors equal $\mathbf{h}_*$, proving (12.2). The inward margin also retains the positive displacement remainder:

$$1 - \mathbf{h}\cdot\mathbf{k} = \tfrac{1}{2}|\mathbf{h}-\mathbf{k}|^2 + \tfrac{1}{2}(1-|\mathbf{k}|^2) \geq \tfrac{1}{2}|\mathbf{h}-\mathbf{k}|^2 + \tfrac{1}{4}\kappa\mathcal{R}. \tag{12.8}$$

Indeed $2\overline{k}_t - D \geq 1$ and $D \geq \kappa\mathcal{R}/2$. □

## 12.2 A sequence of finite Hamilton–Jacobi comparisons

The cell subsolutions give a sequence of comparisons of the whole competitor. The index counts the cells included in the subsolution; the competitor itself is never truncated. For each finite $N$, put

$$\mathcal{Q}_N = \sum_{n=j}^{N} \kappa_n Q_n, \qquad \mathcal{S}_N = t + \sum_{n=j}^{N} \Psi_n, \qquad \mathcal{H}_N(t,x,p_t,p_x) = \tfrac{1}{2}[(p_t - \mathcal{Q}_N)^2 + p_x^2]. \tag{12.9}$$

The calligraphic potential $\mathcal{S}_N$ is distinct from the scalar observation bound $S_N$ in (10.6). Each $\Psi_n$ is constant independently of $x$ outside its cell. Since the cells are disjoint, (12.1) gives

$$\mathcal{H}_N(t,x,d\mathcal{S}_N) \leq \tfrac{1}{2}, \qquad \mathbf{k}^{(N)} = (\partial_t\mathcal{S}_N - \mathcal{Q}_N, \partial_x\mathcal{S}_N) \tag{12.10}$$

on neighborhoods of all attained points. The potentials may be smoothly extended beyond these neighborhoods; no differential bound is asserted there. Equivalently, for every planar velocity $v$,

$$d\mathcal{S}_N(v) \leq |v| + \mathcal{Q}_N v_t.$$

Thus this is a subsolution for the augmented planar length, including negative clock velocities. We construct these subsolutions explicitly; no PDE existence theorem or convergence of the potentials is needed.

**Proposition 12.2** (Finite length comparison)**.** *Suppose the cell subsolutions are defined on neighborhoods of all attained points in cells $j, \dots, N$. Then, including the empty comparison $N = j - 1$,*

$$\Lambda_N = L - L_* + \mathcal{T}_N + \sum_{n=j}^{N} \kappa_n \Delta_n, \tag{12.11}$$

*and every competitor under consideration satisfies*

$$\boxed{L - L_* \geq \Lambda_N - \mathcal{T}_N - C S_N \mathfrak{B}^{11/2}.} \tag{12.12}$$

*In particular, when $L \leq L_*$,*

$$\Lambda_N \leq \mathcal{T}_N + C S_N \mathfrak{B}^{11/2}. \tag{12.13}$$

*Proof.* Integration of (12.10) gives the exact identity

$$L - \Lambda_N = [\mathcal{S}_N] - \int \mathcal{Q}_N \, dt.$$

The endpoint increment is unchanged under repeated or reversed visits. On the reference, the treated cells have zero deficit; on every other cell the comparison is $e_t$, giving deficit $\mathcal{T}_N$. Hence

$$L_* - \mathcal{T}_N = [\mathcal{S}_N] - \int \mathcal{Q}_N(t, f(t)) \, dt.$$

Subtracting proves (12.11). Proposition 10.2 and $\sum_{n=j}^{N} \kappa_n R_n^{\mathrm{obs}} \leq S_N$ give the two inequalities. The same calculation with empty sums includes $N = j - 1$. □

### 12.3 The Hilbert invariant integral for the lifted endpoints

The Hamilton–Jacobi comparison also has an exact integral interpretation in the full space. Using the gap interpolators from (10.5), define

$$\begin{aligned} &\alpha_n = \kappa_n / m_n \quad (j \leq n \leq N), \qquad \alpha_n = 0 \quad \text{otherwise}, \\ &\mu_N = \sum_{n=j}^{N} \alpha_n \zeta_n, \\ &\mathcal{F}_N = \mathcal{S}_N - \int_{-t_j}^{t} \mathcal{Q}_N(u, f(u)) \, du - \mu_N(t)(W - W_*(t)). \end{aligned} \tag{12.14}$$

The multiplier equals $\kappa_n / m_n$ on a treated cell and interpolates only through the tested gaps (Figure 4). It vanishes near zero for each finite $N$, so $\mathcal{F}_N$ is smooth even though $W_*$ is not smooth at zero. Writing $P_W = W - W_*$, differentiation along the horizontal laws gives

$$d\mathcal{F}_N|_{\mathcal{D}_a} = \mathbf{k}^{(N)} \cdot (dt, dx) - (\mu_N \xi^6 + \mu_N' P_W) dt, \qquad \int_\gamma d\mathcal{F}_N = L_* - \mathcal{T}_N. \tag{12.15}$$

Indeed, on a treated cell $\mu_N m_n = \kappa_n$, so the density differences cancel; the endpoint terms containing $\mu_N$ vanish. This is the Hilbert invariant-integral form of the finite comparison: the exact integral is fixed by the lifted endpoints. Summing (10.8) with coefficients $\kappa_n / m_n$ gives

$$\int (\mu_N \xi^6 + \mu_N' P_W) \, dt = -\sum_{n=j}^{N} \kappa_n \Delta_n.$$

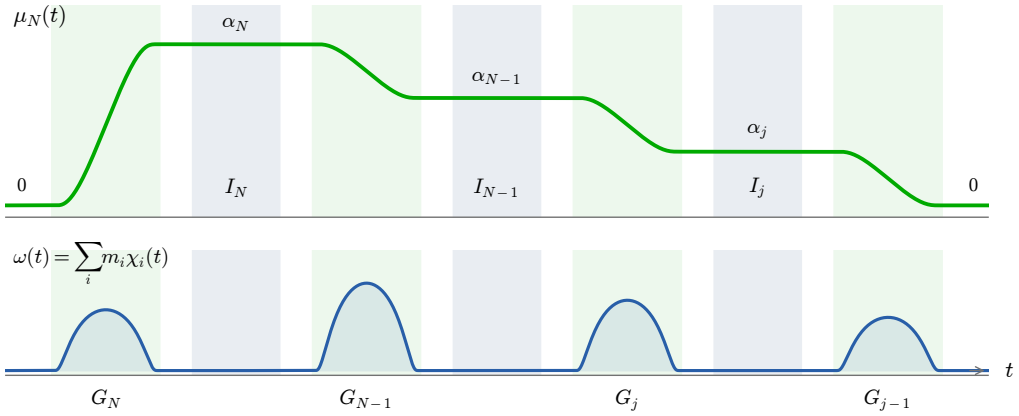


Figure 4: A finite collection of local multipliers joined through the tested gaps. On $I_n$, $\mu_N = \alpha_n = \kappa_n/m_n$. Its derivative is supported where $\omega = \sum_i m_i\chi_i$ records the squared discrepancy $\omega P_W^2 \le \mathcal{E}$. Thus the endpoint observation controls the joining term $\mu_N' P_W$. The picture is schematic; the clock increases to the right and $N = j + 2$.

Substitution recovers (12.11), and the endpoint estimate gives (12.12).

The pointwise Hamilton–Jacobi inequality is for the finite augmented planar problem. The lifted $\mathcal{F}_N$ uses the $Z$-endpoint constraint after integration to control the remaining terms; it is not claimed to satisfy the full six-dimensional eikonal inequality. A single $C^1$ potential sharp along the whole reference, with horizontal gradient norm at most one, would force the unit control to equal that continuous gradient. The reference would then have continuous velocity. The finite subsolutions avoid requiring such a potential.

## 13 Minimality by induction over the cells

We successively bound the fixed clock defect $\mathfrak{B}$ by the reference tail scales. At each stage the old comparison and the endpoint estimate determine the spatial range needed for the next subsolution. The quantity being improved is always the same $\mathfrak{B}$, so its old bound can absorb the new error. The order of choices is fixed: choose the comparison constants, then the attained spatial band, then one small positive $a$, and finally the starting index $j$. None depends on the competitor or on the later induction stage.

**Lemma 13.1** (Induction over the cells)**.** *For sufficiently small fixed $a > 0$ and sufficiently large $j$, every competitor with $L \le L_*$ has defined comparisons through every finite $N$. Moreover,*

$$\mathfrak{B} = 0, \qquad 0 \le \Lambda_N \le \mathcal{T}_N \quad (N \ge j - 1). \tag{13.1}$$

*Proof.* Choose $K > \max\{4, 8C_T\}$ and $M > \max\{1, C_T + 1\}$. Lemma 11.4 gives $C_M$; choose $B_0 > C_M + 1$, then $a > 0$ small enough for that lemma and Lemma 12.1. Let $C_*$ dominate the constants in (10.7) and (12.13). By (10.11), we can choose $j$ so large that

$$C_* K^{11/2} S_n (a^2 h_n)^{9/2} \le \tfrac{1}{2} \qquad (n \ge j). \tag{13.2}$$

Increase $j$ also to meet the bounds on $h_n/\ell_n$ and $\sqrt{h_n/a}/\ell_n$ in the subsolution and spatial estimates. All choices are uniform over competitors.

We prove that the comparison through $N$ is defined and $\mathfrak{B} \le Ka^2 h_{N+1}$. For $N = j - 1$, the empty comparison is defined, and (9.1) and Lemma 9.1 give $\mathfrak{B} \le 2\Lambda_{j-1} \le 2C_T a^2 h_j$. Suppose the

assertion holds through $n-1$. Apply (12.13) to this old comparison:

$$\Lambda_{n-1} \le C_T a^2 h_n + C_* S_{n-1} (K a^2 h_n)^{11/2} \le (C_T + \tfrac{1}{2}) a^2 h_n < M a^2 h_n.$$

Here $S_{n-1} \le S_n$ and (13.2) give the second inequality. Independently, the endpoint estimate and (10.12) give

$$\kappa_n \Delta_n \le C_* S_n (K a^2 h_n)^{11/2} \le \tfrac{1}{2} a^2 h_n = \kappa_n \nu_n h_n.$$

Thus both hypotheses of Lemma 11.4 hold before the new comparison is introduced. All visits to $I_n$ lie in $\mathcal{G}_n \le C_M < B_0$, so its subsolution is now available.

For this new comparison, (9.10) and (12.13) imply

$$\mathfrak{B} \le 4\Lambda_n \le 4C_T a^2 h_{n+1} + 4C_* S_n \mathfrak{B}^{11/2}. \tag{13.3}$$

The inductive bound on the same fixed quantity $\mathfrak{B}$ gives

$$4C_* S_n \mathfrak{B}^{11/2} \le 4C_* S_n (K a^2 h_n)^{9/2} \mathfrak{B} \le \frac{2}{K} \mathfrak{B} \le \tfrac{1}{2} \mathfrak{B}.$$

Absorbing yields $\mathfrak{B} \le 8C_T a^2 h_{n+1} \le K a^2 h_{n+1}$, completing the induction. Since $h_{N+1} \to 0$, we obtain $\mathfrak{B} = 0$. Equation (12.13) then gives (13.1). □

*Proof of Proposition 7.1.* Take a competitor of length $L \le L_*$ and parametrize it by planar arclength. The finite stages of Lemma 13.1 give the explicit verification estimate

$$L - L_* \ge \Lambda_N - \mathcal{T}_N - \delta_N, \qquad \delta_N = C S_N (K a^2 h_{N+1})^{11/2} \longrightarrow 0. \tag{13.4}$$

Indeed, (10.10) and $h_{N+1} \le h_N$ give

$$\delta_N \le C_K a^9 h_{N+1}^{5/4} \longrightarrow 0, \qquad \mathcal{T}_N \le C_T a^2 h_{N+1} \longrightarrow 0.$$

Thus the nonnegative deficits prove $L = L_*$. The argument passes to a limit of comparison inequalities on the same competitor, not to a limit of the potentials. The lemma also gives $\Lambda_N \to 0$, which we now use for uniqueness.

On each fixed cell its nonnegative contribution to $\Lambda_N$ is independent of $N$ once that cell is included, so that contribution is zero. The deficit relative to $e_t$ off the cells is also zero. Since $|\mathbf{k}_n| \le 1$, equality $1 - \mathbf{h} \cdot \mathbf{k}_n = 0$ implies $\mathbf{h} = \mathbf{k}_n$ and $|\mathbf{k}_n| = 1$. Every comparison clock component is at least $3/4$, so the clock is strictly increasing with a Lipschitz inverse.

Reparametrize by $t$. On each treated cell the vanishing deficit gives

$$\frac{dx}{dt} = \frac{(\mathbf{k}_n)_x(t,x)}{(\mathbf{k}_n)_t(t,x)}.$$

The right-hand side is smooth on the attained open sublevel and its denominator is at least $3/4$. By (12.2), $x = f(t)$ solves the same equation. Off the cells, both satisfy $dx/dt = 0$. For any $\delta > 0$, only finitely many cells meet $[\delta, T_j]$; their comparisons equal $e_t$ near their boundaries. Starting from the common terminal value $x(T_j) = f(T_j) = 0$, local ODE uniqueness backwards through these cells and gaps gives $x = f$ on $[\delta, T_j]$. Letting $\delta \downarrow 0$ and using continuity proves equality for positive clocks and at zero. On the negative part the initial endpoint and $dx/dt = 0$ identify the graph.

Uniqueness for the auxiliary equations then identifies the entire horizontal lift.

In an arbitrary original parameter, equality means

$$\eta = \gamma \circ \theta, \qquad \theta : [0,T] \longrightarrow [s(-t_j), s(T_j)]$$

for a continuous nondecreasing map with the prescribed endpoint values. Thus $L \le L_*$ forces equality and this reparametrization. A shorter replacement for a subarc would shorten the full arc by splicing. An equal-length replacement is likewise identified by the full-arc uniqueness. □

### 13.1 The counterexample

The geometric properties and the length comparison now give the main theorem.

*Proof of Theorem 1.* Choose a sufficiently small $a > 0$ as in Proposition 7.1. By Proposition 8.1, (6.24) is a smooth bracket-generating orthonormal frame on a neighborhood of zero. Choose a relatively compact open set $\Omega$ whose closure lies in that neighborhood. For sufficiently large $j$, the reference segment $\Gamma_a([-t_j, 7t_j/4])$ lies in $\Omega$. Proposition 7.1 gives uniqueness of the length minimizer there, up to reparametrization, and the same property for each subarc. Corollary 8.13 gives the velocity discontinuity at the interior point zero. Strict abnormality follows from Proposition 8.1. □

## 14 Further properties and equiregular lifting

We collect the remaining properties of the frame and the reference arc. They hold throughout the range $0 < a \le 1/4$, independently of the length comparison. We then give an equiregular lift for the minimizing arcs of Theorem 1.

A tangent at an interior point is a locally uniform limit of rescaled arcs in the nilpotent approximation at that point. More precisely, take privileged coordinates centered at the point, with dilations $\delta_r(z)_k = r^{w_k} z_k$ of the corresponding weights $w_k$. One considers the limits of $\delta_{1/r}\gamma(s_0 + r\,\cdot)$ along sequences $r \downarrow 0$, writing the curve in these coordinates. The set of all limits is the tangent cone. A horizontal line in the approximation is the integral curve through the base point with constant unit control [20].

**Proposition 14.1.** *For $0 < a \le 1/4$, the construction has the following properties. Let $u$ be the arclength control of $\Gamma_a$ in the defining orthonormal frame, with $s = 0$ at the origin, and put $e_t = (1, 0)$.*

*(i) No smooth local diffeomorphism at zero carries $\mathcal{D}_a$ to a real-analytic distribution. In particular, no smooth local coordinates near zero give it a polynomial horizontal frame.*

*(ii) The degree of nonholonomy at zero, namely the least bracket length needed to span the tangent space, is exactly 51. The dimension of the span of $\mathcal{D}_a$ and its first brackets is nonconstant on every neighborhood of zero. No local frame of $\mathcal{D}_a$ near zero generates a Lie algebra with abelian derived algebra.*

*(iii) The arclength parametrization of $\Gamma_a$ is smooth away from zero and differentiable at zero. Its control satisfies $u(r\,\cdot) \to e_t$ in $L^2_{\mathrm{loc}}(\mathbb{R})$ as $r \downarrow 0$, and its tangent cone at zero consists of one horizontal line.*

*(iv) Let $\gamma$ be the arclength parametrization of $\Gamma_a$. The cotangent curve $s \mapsto dZ_{\gamma(s)}$ is an abnormal extremal over $\gamma$, and each covector $dZ_{\gamma(s)}$ annihilates $(\mathcal{D}_a + [\mathcal{D}_a, \mathcal{D}_a])_{\gamma(s)}$.*

*(v) Restrict $u$ to a sufficiently small interval about zero whose endpoints lie in straight portions of the reference, and extend it by $e_t$. For $1 < p < \infty$,*

$$\|u(\,\cdot + \delta) - u\|_{L^p(\mathbb{R})} \le C_p a |\delta|^{1/p}, \qquad 0 < |\delta| < 1.$$

*For $p = 1$, the bound is*

$$\|u(\,\cdot + \delta) - u\|_{L^1(\mathbb{R})} \le C a |\delta| (1 + \sqrt{\log\log(e^e/|\delta|)}).$$

**Lemma 14.2** (Flat decay of the Levi bracket)**.** *Let $\mathcal{L}$ denote the Levi bracket of $\mathcal{D}_a$, and set $\Sigma = \{p : \mathcal{L}_p = 0\}$. For $p_h = (-h, 0, 0, 0, 0, 0)$, $h > 0$ sufficiently small, the coordinate Euclidean norms and distance satisfy*

$$\|\mathcal{L}_{p_h}\| = e^{-1/h^2}, \qquad \operatorname{dist}(p_h, \Sigma) = h. \tag{14.1}$$

*Proof.* For a smooth distribution $\mathcal{D}$, its Levi bracket at $p$ is the linear map

$$\mathcal{L}_p : \bigwedge\nolimits^2 \mathcal{D}_p \longrightarrow T_pM/\mathcal{D}_p, \qquad v \wedge w \longmapsto [V, W](p) \bmod \mathcal{D}_p,$$

where $V, W$ are local horizontal fields extending $v, w$. The class of the bracket is independent of the extensions. Write $\Sigma = \{p : \mathcal{L}_p = 0\}$. Both the tensor and its zero set are preserved under smooth equivalences of distributions.

Let $B = [X_1, X_2]$. Since $X_1, X_2$ project to the commuting coordinate fields in the plane, $B$ is vertical. The horizontal plane is transverse to the vertical space, so $\Sigma = \{p : B(p) = 0\}$. On the negative clock half-space, $q = -x^4/2$ and $e = 0$. The $r$- and $\xi$-components of the bracket are

$$B(r) = -6x^2, \qquad B(\xi) = -\rho_-(t) = -e^{-1/t^2} < 0.$$

Thus $\Sigma$ has no points with negative clock coordinate. Also $0 \in \Sigma$, by (8.19) and Lemma 8.10.

Put $p_h = (-h, 0, 0, \dots, 0)$, $h > 0$. On the negative clock half-space the cell cutoffs vanish and $q(t, x) = -x^4/2$. At $p_h$ the only nonzero component of $B$ is therefore $B(\xi) = -e^{-1/h^2}$, by (6.24). At this point $X_1 = \partial_t$ and $X_2 = \partial_x$. Use the coordinate Euclidean metric, its induced norms on $\bigwedge^2 \mathcal{D}_a$ and $TM/\mathcal{D}_a$, and its ordinary distance to $\Sigma$. Because the origin is at distance $h$ from $p_h$ and every point of $\Sigma$ has nonnegative clock coordinate, we obtain (14.1). □

*Proof of Proposition 14.1*(i). For a real-analytic distribution its Levi tensor has real-analytic components $F_1, \dots, F_k$ in local analytic bundle frames. Their common zero set is $\Sigma$, and their Euclidean norm is locally comparable to the chosen smooth norm of the Levi tensor. Apply the Łojasiewicz distance inequality to $\sum_j F_j^2$ and take square roots [9, Corollary 4(2) and Remark 1.4]. Near any point of $\Sigma$ this gives constants $c, N > 0$ such that

$$\|\mathcal{L}_p\| \;\geq\; c \operatorname{dist}(p, \Sigma)^N. \tag{14.2}$$

The existence of such a bound is invariant under smooth local diffeomorphisms. Indeed, a diffeomorphism transports the Levi tensor and its zero set. After restricting the neighborhood it is bi-Lipschitz for ordinary coordinate distances, and the induced maps on the tensor fibers and their inverses have bounded norms. Thus a real-analytic realization of $\mathcal{D}_a$ would give (14.2) in the original coordinates, possibly with a different constant $c$. But (14.1) gives $e^{-1/h^2}/h^N \to 0$ for every $N > 0$. This contradiction rules out such a realization. A polynomial frame would give a real-analytic distribution in its coordinate chart. The base germ admits no subanalytic realization either. Indeed, if the smooth map $p \mapsto \mathcal{D}_{a,p}$ to the Grassmannian were subanalytic in some smooth coordinates, its components in a Grassmannian chart would be smooth subanalytic functions, hence real-analytic by Tamm's theorem [26, Theorem 2.3.3(i)]. □

*Proof of Proposition 14.1*(ii). The brackets in Subsection 8.4 have lengths 4 for $T$, 5 for $V_0$, and $5d + 1$ for $\operatorname{ad}_{V_0}^d X_1^0$. The following weights show that these directions occur at their first possible orders.

| Coordinate | $t$ | $x$ | $r$ | $\zeta$ | $W$ | $Z$ |
|---|---|---|---|---|---|---|
| Weight | 1 | 1 | 4 | 5 | 31 | 51 |

The fields $X_1^0, X_2^0$ are homogeneous of weighted degree $-1$, so a bracket of length $k$ is homogeneous of degree $-k$. Its value at zero in a coordinate direction of weight $w$ can therefore be nonzero only if $k = w$. Flat additions do not change bracket values at zero. Combining this lower bound with the brackets already constructed gives

$$\dim \mathcal{D}^k(0) = 2 + \#\{w \in \{4, 5, 31, 51\} : w \le k\}, \qquad k \ge 1,$$

where $\mathcal{D}^k$ is the span of brackets of length at most $k$. In particular, the degree of nonholonomy is exactly 51. The same degree argument shows that every composition of fewer than $w$ horizontal fields annihilates a coordinate of weight $w$ at zero. The bracket producing that direction at length $w$ shows that some composition of exactly $w$ fields does not. Thus the coordinates are privileged, with the displayed weights, and $(X_1^0, X_2^0)$ is the nilpotent approximation.

The growth already varies at the first bracket. At zero, $[X_1, X_2](0) = 0$. At every point $\Gamma_a(t)$ with $t < 0$, the $\xi$-component of $[X_1, X_2]$ is $-\rho_-(t) < 0$. The bracket has zero projection onto the $(t, x)$-plane, while the frame projects to its coordinate basis. Thus, for $t \le 0$,

$$\dim(\mathcal{D}_a + [\mathcal{D}_a, \mathcal{D}_a])_{\Gamma_a(t)} = \begin{cases} 2, & t = 0, \\ 3, & t < 0. \end{cases}$$

In particular, the distribution is not locally equivalent near zero to the horizontal distribution of a Carnot group.

It is also non-metabelian in the sense of [13, Definition 3.2]. To check the intrinsic statement, first put $B_0 = [X_1^0, X_2^0]$. Direct computation gives

$$[B_0, [X_1^0, B_0]]\, W = 180 x^6 (\zeta - x^5/10)^4 \not\equiv 0.$$

Thus its generated Lie algebra has nonabelian derived algebra. If the original distribution admitted a metabelian local frame, all brackets between words of length at least two in that frame would vanish identically. Rescaling in the privileged coordinates passes these identities to the leading homogeneous frame. That frame is an invertible constant linear recombination of $X_1^0, X_2^0$, and therefore generates the same polynomial Lie algebra. This contradicts the displayed computation. This last argument is necessary: failure of the metabelian identities in one chosen frame, by itself, would not exclude another frame. □

*Proof of Proposition 14.1*(iii). The reference and its arclength parametrization are smooth away from zero, where the defining profiles and coefficients are smooth. We prove differentiability at zero and identify the tangent using the control estimates. For $t_j/2 \le t \le t_j$, (9.3) and the separation of scales give

$$0 \le s(t) - t \le Ca^2 \sum_{n \ge j} (h_n + h_n^2/\ell_n) \le C' a^2 h_j, \qquad \int_0^{s(t)} |u - e_t|^2 \, ds = 2(s(t) - t).$$

The identity follows from $|u| = 1$ and $u_1 = dt/ds$. Since $h_j/t_j \to 0$ and the negative half is straight, for each $R > 0$ we have

$$\frac{1}{r} \int_{-rR}^{rR} |u - e_t|^2 \, ds \longrightarrow 0.$$

Integrating the control equation in a smooth frame gives $\gamma'(0) = X_1(0)$. Equivalently, in a privileged coordinate chart the rescaled fields converge locally with their derivatives to their nilpotent approximations. The integral control equation and Gronwall's inequality, using the strong $L^1$ convergence of the controls on compact intervals, give the unique constant-control integral curve in that approximation. This is a horizontal line in the sense of [19, 20].

The smooth frame identifies a limiting control $(v_1, v_2)$ with the horizontal vector $v_1X_1(0) + v_2X_2(0)$. Thus the arc of right-hand velocity limits from Corollary 8.13 has the tangent vector $X_1(0)$ as one endpoint. □

*Proof of Proposition 14.1*(iv). Subsection 8.4 identifies $s \mapsto dZ_{\gamma(s)}$ as an abnormal extremal. Along $\gamma$, we also have

$$[X_1, X_2]Z = X_1(X_2Z) - X_2(X_1Z) = 0,$$

because $d(X_1Z) = 0$ there and $X_2Z = 0$ identically. The extremal thus satisfies the Goh annihilation condition. □

**Lemma 14.3** (Translation of a single pulse)**.** *Let $q_n = u - e_t$ on the arclength image of $I_n$, extended by zero. For $1 \le p < \infty$ and $0 < |\delta| < 1$,*

$$\|q_n(\cdot + \delta) - q_n\|_p^p \le C_p a^p \min\{|\delta|^p h_n^{1-p},\, h_n\}.$$

*Proof.* For the full pulse $q_n$, the profile bounds and the cutoff scale give, for each $p \ge 1$,

$$\|q_n\|_p^p \le C_p a^p h_n, \qquad \|q_n'\|_p^p \le C_p a^p h_n^{1-p}.$$

Indeed $q_n$ is obtained from $f_n'$ by the smooth map $z \mapsto (1, z)/\sqrt{1 + z^2} - e_t$, which vanishes at zero. Its derivatives are bounded on the range of $f_n'$. Since $ds/dt = \sqrt{1 + f_n'^2}$ is bounded above and below, the pulse and its derivative can be estimated in clock time. On differentiating $b_n\beta_n F_{a,n}$, the terms containing derivatives of $F_{a,n}$ are integrated using Lemma 8.4 at scale $h_n$. The terms with all derivatives falling on $\beta_n$ contribute at most

$$C_p a^p h_n^p \ell_n^{1-p} \quad \text{and} \quad C_p a^p h_n^p \ell_n^{1-2p},$$

respectively. Since $h_n \le \ell_n$, these are bounded by the claimed powers of $h_n$. For the translation, use both

$$\|q_n(\cdot + \delta) - q_n\|_p \le |\delta|\, \|q_n'\|_p, \qquad \|q_n(\cdot + \delta) - q_n\|_p \le 2\|q_n\|_p.$$

□

*Proof of Proposition 14.1*(v). The full control satisfies $u - e_t = \sum_n q_n$; the supports of the pulses are disjoint in arclength. Apply Lemma 14.3 to each summand. At any point at most two terms in the translated sum are nonzero. For $p > 1$, splitting at $h_n = |\delta|$ and using $h_{n+1} \le h_n/2$ bounds the sum by $C_p a^p |\delta|$. For $p = 1$, the pulses with $h_n \ge |\delta|$ contribute at most $Ca|\delta|$ each. Their number is at most $1 + \sqrt{\log\log(1/|\delta|)}$ for small $|\delta|$, by the definition of $h_n$. The sum of the remaining transition scales, those with $h_n < |\delta|$, is at most $2|\delta|$. If the control is restricted to the interval in the statement and extended by $e_t$, the centered control is multiplied by the indicator of that interval. On the intersection of the interval and its translate the difference is the original one. On their symmetric difference, of length at most $2|\delta|$, it has size at most $Ca$. Thus the two endpoints contribute at most $C_p a^p |\delta|$ to the $p$-th power of the norm. This gives both estimates for the restricted control. □

For every fixed $\eta > 0$, Proposition 14.1(iii) gives

$$\big|\{s \in [-r, r] : |u(s) - e_t| \ge \eta\}\big| \le \eta^{-2} \int_{-r}^{r} |u - e_t|^2\, ds = o(r).$$

Thus the times with a fixed nonzero velocity deviation have vanishing density at zero. For fixed $R > 0$, the window $|t - t_n| \le Rh_n$ occupies a fraction $Rh_n/\ell_n \to 0$ of the cell in clock time, while the velocity at its center has the same value for every $n$ by (8.13).

**Remark 14.4** (Regularity of the reference primitive)**.** *Subsection 4.3 shows that $W_*$ fails to be $C^6$ on every neighborhood of zero. Its gap values $w_n$ nevertheless define smooth coefficients, and its local absolute continuity suffices in (10.8). The finite Hilbert potential (12.14) multiplies it by $\mu_N$, which vanishes near zero, and is therefore smooth.*

### 14.1 Relation to regularity theorems

In terms of the arclength control $u$, the tangent-line theorem gives, at each interior time $s_0$, a sequence $r_k \downarrow 0$ and a unit vector $v$ such that $u(s_0 + r_k\,\cdot) \to v$ in $L^2_{\mathrm{loc}}(\mathbb{R})$ [19, Remark 4.3]. Every blow-up also minimizes on compact intervals in the nilpotent approximation [20, Theorem 3.6]. For the minimizer of Theorem 1, Proposition 14.1(iii) gives convergence to the same horizontal line along every sequence of scales at the origin. Its velocity has a left limit there and no right limit, so the discontinuity is compatible with the exclusion of corners. The structure lies outside the hypotheses of the following $C^1$ regularity theorems.

Barilari, Chitour, Jean, Prandi and Sigalotti prove $C^1$ regularity for rank-two structures of step at most four [4, Corollary 2]. Here the degree at zero is 51. Belotto da Silva, Figalli, Parusiński and Rifford prove $C^1$ regularity in analytic three-dimensional structures [5]. Le Donne, Paddeu and Socionovo prove it for analytic, equiregular, metabelian rank-two structures [13, Theorem 1.1]. Proposition 14.1(i) excludes smooth local equivalence of the six-dimensional distribution to any real-analytic distribution. Its growth is nonconstant, and it is non-metabelian.

Socionovo's analysis of the polynomial family containing the seven-author example provides explicit shortenings of certain rigid abnormal extremal trajectories [23, Theorem 1.2 and Corollary 1.4]. It is a useful reminder that rigidity and minimality require different arguments.

Lokutsievskiy and Zelikin prove $L^p$-Hölder regularity of minimizer derivatives in the constant-rank setting [15, Theorem 1]. Proposition 14.1(v) gives a direct estimate for this reference, independently of minimality.

### 14.2 Equiregular lifting

The nonconstant growth of the six-dimensional realization can be removed by lifting the structure to a higher-dimensional space. Here equiregularity means that the dimensions of the spans of brackets of each bounded length are constant.

**Proposition 14.5.** *There exists a smooth, equiregular, bracket-generating rank-two sub-Riemannian structure admitting a length-minimizing curve whose arclength velocity is discontinuous at an interior point. Its arclength parametrization is a strictly abnormal extremal trajectory.*

*Proof of Proposition 14.5.* Fix $0 < a \le a_0$, with $a_0$ as in Proposition 7.1. By Propositions 8.1 and 14.1(ii), the fields $X_1, X_2$ define a smooth bracket-generating structure near zero, with degree of nonholonomy 51 at zero. Let $\mathfrak{f}_{2,51}$ be the free nilpotent Lie algebra on two generators of step 51, and put $N = \dim \mathfrak{f}_{2,51}$. Jean's desingularization theorem [12, Lemma 2.5] gives neighborhoods $U \subset \mathbb{R}^6$ and $\widetilde{U} \subset U \times \mathbb{R}^{N-6}$ of zero and $(0,0)$, respectively, and smooth vector fields $\widetilde{X}_1, \widetilde{X}_2$ on $\widetilde{U}$ such that

$$d\pi(\widetilde{X}_i) = X_i \circ \pi, \qquad i = 1, 2,$$

where $\pi$ is the coordinate projection. The lifted fields are free up to step 51 and bracket-generating throughout $\widetilde{U}$. Declaring them orthonormal gives a smooth equiregular rank-two structure, and $d\pi$ is an isometry on each horizontal plane.

Let $\gamma$ be the arclength parametrization of the reference, with $\gamma(0) = 0$ and unit control $u = (u_1, u_2)$. Starting at $(0,0)$, solve in both time directions

$$\dot{\widetilde{\gamma}}(s) = u_1(s)\widetilde{X}_1(\widetilde{\gamma}(s)) + u_2(s)\widetilde{X}_2(\widetilde{\gamma}(s)).$$

Uniqueness for the control equation gives $\pi \circ \widetilde{\gamma} = \gamma$, with the same arclength parameter. For sufficiently large $j$, the reference arc from Proposition 7.1 and this lift stay in $U$ and $\widetilde{U}$. Every

horizontal competitor $\widetilde{\eta}$ with the lifted endpoints projects to a competitor for that reference arc. Since projection preserves horizontal length,

$$L(\widetilde{\eta}) = L(\pi \circ \widetilde{\eta}) \geq L(\gamma) = L(\widetilde{\gamma}).$$

The lift therefore minimizes length.

If $\widetilde{\gamma}$ were $C^1$ near zero, its smooth projection $\gamma$ would be $C^1$ there, contrary to Proposition 8.1. On each subinterval containing zero in its interior, $\widetilde{\gamma}$ minimizes length, so the Pontryagin maximum principle supplies an extremal over it [1, 2, 21]. Every normal extremal has a smooth arclength projection. Hence on each such subinterval $\widetilde{\gamma}$ is a strictly abnormal extremal trajectory. □

For this free lifting, the Witt dimension formula gives

$$N = \sum_{k=1}^{51} \frac{1}{k} \sum_{d|k} \mu(d)\, 2^{k/d} \approx 9.0149 \times 10^{13},$$

where $\mu$ is the Möbius function. This is a sufficient dimension, not a lower bound for an equiregular realization. The lifted structure has constant free graded symbol. Its degree-two layer is nonzero everywhere, so its Levi bracket has no zeros. The length-preserving projection argument above also appears in the regularity reduction of [4, Section 3.1, proof of Lemma 7].

**Analyticity of the lift.** Every horizontally isometric lift in Proposition 14.5 has a sub-Riemannian germ over the origin that admits no real-analytic realization. The obstruction is visible along the clock flow. Let $\phi_s$ be the flow of $X_1$. For $s < 0$, transport $X_2$ back to the origin along the flow. Its $\xi$-component is

$$d\xi\Big((d\phi_s|_0)^{-1} X_2(\phi_s(0))\Big) = -\int_0^s \rho_-(u)\, du.$$

This component is nonzero for $s < 0$ and flat at zero. Upstairs the pullback of the clock has unit horizontal gradient $\widetilde{X}_1$. Its flow is the projection of the normal Hamiltonian flow starting on the graph of $d(t \circ \pi)$ [1]. If the lifted structure were analytic, the clock line and the differential of the lifted clock flow at its initial point would depend analytically on $s$. For the differential, only the first jet of the initial covector field at that point enters. The perpendicular horizontal unit vector with a fixed choice of sign would also be analytic along this line. Transporting it back to the initial point and applying the fixed linear map $d\pi$ there would force the flat component above to be analytic.

The free lift can also be chosen so that its plane field alone admits no real-analytic realization. The homogeneous fields (8.19) generate a transitive local action of the free rank-two, step-51 group $G$, so their model is locally $K\backslash G$, with $K$ the stabilizer of the origin. Adding $K$-invariant lifts of the flat perturbations $X_i - X_i^0$ to the left-invariant generators preserves their jets at the identity. The lift is therefore free nearby, and its fibers are orbits of distribution symmetries. The free symbol has finite Tanaka prolongation [8]. If the lifted plane field were analytic, the infinitesimal generators of these orbits would be analytic [29, Theorem 4.1], so the local quotient would give a real-analytic realization of the base, contrary to Proposition 14.1(i). Whether the plane field of an arbitrary free lift must be intrinsically nonanalytic after one forgets the metric and the projection is unsettled. The existence of a minimizer with discontinuous arclength velocity for a left-invariant metric on a Carnot group remains open.

## References

[1] A. Agrachev, D. Barilari and U. Boscain, *A Comprehensive Introduction to Sub-Riemannian Geometry*, Cambridge Studies in Advanced Mathematics, vol. 181, Cambridge University Press, Cambridge, 2020. doi:10.1017/9781108677325.

[2] A. A. Agrachev and Yu. L. Sachkov, *Control Theory from the Geometric Viewpoint*, Encyclopaedia of Mathematical Sciences, vol. 87, Springer-Verlag, Berlin, 2004. doi:10.1007/978-3-662-06404-7.

[3] A. A. Agrachev and A. V. Sarychev, *Strong minimality of abnormal geodesics for 2-distributions*, J. Dynam. Control Systems **1** (1995), 139–176.

[4] D. Barilari, Y. Chitour, F. Jean, D. Prandi and M. Sigalotti, *On the regularity of abnormal minimizers for rank 2 sub-Riemannian structures*, J. Math. Pures Appl. **133** (2020), 118–138. arXiv:1804.00971.

[5] A. Belotto da Silva, A. Figalli, A. Parusiński and L. Rifford, *Strong Sard conjecture and regularity of singular minimizing geodesics for analytic sub-Riemannian structures in dimension 3*, Invent. Math. **229** (2022), 395–448. doi:10.1007/s00222-022-01111-2.

[6] N. Cavallucci, E. Le Donne and S. Nicolussi Golo, *Carnot geodesics with Hölder controls*, preprint, 2026. arXiv:2610.38481.

[7] Y. Chitour, F. Jean, R. Monti, L. Rifford, L. Sacchelli, M. Sigalotti and A. Socionovo, *Not all sub-Riemannian minimizing geodesics are smooth*, preprint, 2025. arXiv:2501.18920.

[8] B. Doubrov and O. Radko, *Graded nilpotent Lie algebras of infinite type*, J. Lie Theory **20** (2010), no. 3, 525–541. arXiv:1001.0379.

[9] P. M. N. Feehan, *Resolution of singularities and geometric proofs of the Łojasiewicz inequalities*, Geom. Topol. **23** (2019), no. 7, 3273–3313. arXiv:1708.09775.

[10] E. Hakavuori and E. Le Donne, *Non-minimality of corners in subriemannian geometry*, Invent. Math. **206** (2016), no. 3, 693–704. doi:10.1007/s00222-016-0661-9. arXiv:1509.05578.

[11] D. Hilbert, *Mathematical problems*, translated by M. W. Newson, Bull. Amer. Math. Soc. **8** (1902), no. 10, 437–479. doi:10.1090/S0002-9904-1902-00923-3.

[12] F. Jean, *Control of Nonholonomic Systems: from Sub-Riemannian Geometry to Motion Planning*, SpringerBriefs in Mathematics, Springer, Cham, 2014. doi:10.1007/978-3-319-08690-3.

[13] E. Le Donne, N. Paddeu and A. Socionovo, *Metabelian distributions and sub-Riemannian geodesics*, Adv. Calc. Var. **19** (2026), no. 3, 423–433. doi:10.1515/acv-2025-0104. arXiv:2405.14997.

[14] W. Liu and H. J. Sussmann, *Shortest paths for sub-Riemannian metrics on rank-two distributions*, Mem. Amer. Math. Soc. **118** (1995), no. 564, x+104 pp. doi:10.1090/memo/0564.

[15] L. Lokutsievskiy and M. Zelikin, *Derivatives of sub-Riemannian geodesics are $L_p$-Hölder continuous*, ESAIM Control Optim. Calc. Var. **29** (2023), article 70. doi:10.1051/cocv/2023055.

[16] R. Montgomery, *Abnormal minimizers*, SIAM J. Control Optim. **32** (1994), no. 6, 1605–1620. doi:10.1137/S0363012993244945.

[17] R. Montgomery, *A Tour of Subriemannian Geometries, Their Geodesics and Applications*, Mathematical Surveys and Monographs, vol. 91, American Mathematical Society, Providence, RI, 2002. doi:10.1090/surv/091.

[18] R. Monti, *The regularity problem for sub-Riemannian geodesics*, in *Geometric Control Theory and Sub-Riemannian Geometry*, Springer INdAM Series **5** (2014), 313–332.

[19] R. Monti, A. Pigati and D. Vittone, *Existence of tangent lines to Carnot–Carathéodory geodesics*, Calc. Var. Partial Differential Equations **57** (2018), no. 3, article 75. doi:10.1007/s00526-018-1361-7. arXiv:1609.07261.

[20] R. Monti, A. Pigati and D. Vittone, *On tangent cones to length minimizers in Carnot–Carathéodory spaces*, SIAM J. Control Optim. **56** (2018), 3351–3369. doi:10.1137/17M114056X.

[21] L. S. Pontryagin, V. G. Boltyanskii, R. V. Gamkrelidze and E. F. Mishchenko, *The Mathematical Theory of Optimal Processes*, translated by K. N. Trirogoff, edited by L. W. Neustadt, Interscience Publishers, New York, 1962.

[22] T. Rossi, A. J. A. Schiavoni Piazza and A. Socionovo, *Interior singularity and branching of geodesics in real-analytic sub-Riemannian manifolds*, preprint, 2026. arXiv:2603.23068.

[23] A. Socionovo, *Sharp regularity of sub-Riemannian length-minimizing curves*, Calc. Var. Partial Differential Equations **65** (2026), article 181. doi:10.1007/s00526-026-03343-z. arXiv:2502.00403v2.

[24] R. S. Strichartz, *Sub-Riemannian geometry*, J. Differential Geom. **24** (1986), no. 2, 221–263. doi:10.4310/jdg/1214440436.

[25] R. S. Strichartz, *Corrections to: "Sub-Riemannian geometry"*, J. Differential Geom. **30** (1989), no. 2, 595–596. doi:10.4310/jdg/1214443604.

[26] M. Tamm, *Subanalytic sets in the calculus of variation*, Acta Math. **146** (1981), 167–199. doi:10.1007/BF02392462.

[27] B. Wang and I. Zelenko, *Hölder exponents for the velocity of minimizers in rank-two Carnot groups*, manuscript in preparation, November 2026.

[28] I. Zelenko, *Nonregular abnormal extremals of 2-distribution: existence, second variation, and rigidity*, J. Dynam. Control Systems **5** (1999), 347–383.

[29] I. Zelenko, *On Tanaka's prolongation procedure for filtered structures of constant type*, SIGMA **5** (2009), article 094, 21 pp. doi:10.3842/SIGMA.2009.094.

[30] M. I. Zelikin and L. V. Lokutsievskiy, *Finsler and sub-Finsler geodesics with chattering*, Proc. Steklov Inst. Math. **332** (2026), 91–107. doi:10.1134/S0081543826600523. arXiv:2505.24474.

Bangjie Wang
Department of Mathematics
Texas A&M University
College Station, Texas, USA
*Email address*: bangjiewang@tamu.edu
*URL*: https://sites.google.com/view/bangjie-wang/home?pli=1&authuser=0

Igor Zelenko
Department of Mathematics
Texas A&M University
College Station, Texas 77843, USA
*Email address*: zelenkotamu@tamu.edu
*URL*: https://people.tamu.edu/~zelenkotamu/